

Copyright © 2023 SEPM Society for Sedimentary Geology. The author accepted manuscript is made available on this institutional repository under a Creative Commons (CC BY) Attribution License (<https://creativecommons.org/licenses/by/4.0/> - see: <https://www.sepm.org/publication-permissions>).

Owen, A. , Hartley, A. J., Hoey, T. B., Ebinghaus, A., Jolley, D. W. and Weissmann, G. S. (2023) Analysis of the fluvial stratigraphic response to the Paleocene–Eocene Thermal Maximum in the Bighorn Basin, U.S.A. *Journal of Sedimentary Research*, 93(5), pp. 293-308. (doi: [10.2110/jsr.2021.134](https://doi.org/10.2110/jsr.2021.134))

There may be differences between this version and the published version. You are advised to consult the publisher's version if you wish to cite from it.

1 **Analysis of the Fluvial Stratigraphic Response to the Paleocene-Eocene Thermal Maximum in the**  
2 **Bighorn Basin, USA**

3 **Amanda Owen<sup>1</sup>, Adrian J. Hartley<sup>2</sup>, Trevor B. Hoey<sup>3</sup>, Alena Ebinghaus<sup>2</sup>, David W. Jolley<sup>2</sup>, and Gary S.**  
4 **Weissmann<sup>4</sup>**

5 *<sup>1</sup>School of Geographical and Earth Sciences, University of Glasgow, G12 8QQ, UK*

6 *<sup>2</sup>Department of Geology and Petroleum Geology, University of Aberdeen, AB24 3UE, UK*

7 *<sup>3</sup>Department of Civil and Environmental Engineering, Brunel University London, Uxbridge, UB8 3PH, UK*

8 *<sup>4</sup>Department of Earth and Planetary Sciences, University of New Mexico, New Mexico, 87131-0001, USA*

9 **ABSTRACT**

10 Geological deposits can reveal how environments of the past have responded to climate change,  
11 enabling important insights into how environments may respond to our current anthropogenically  
12 induced warming. The Paleocene-Eocene Thermal Maximum (PETM) occurred ca. 56 Ma and was a  
13 short-lived (approximately 200,000 years) global warming event (5-8°C rise). The PETM has been  
14 investigated at several terrestrial and marine localities across the globe. However, many studies are  
15 based on single successions, with very few sites being placed within a well-defined spatial and temporal  
16 context and with comparisons limited to deposits that lie immediately above and below the event. Due  
17 to the inherent variability of sedimentary systems, it is imperative that the appropriate context is  
18 provided to fully understand the impacts of climate change on landscapes and subsequent deposits. This  
19 study examines 28 locations, totaling over 4 km of recorded stratigraphy, within a newly defined  
20 quantified sedimentary basin context (Bighorn Basin, USA) to evaluate variability of fluvial response to  
21 the PETM. We show that channel-body and story thicknesses across the PETM are not statistically

22 significantly different from deposits outside the climate event, implying that there is not a consistent  
23 sedimentary response to the climate event across the basin. Based on our large dataset we calculate  
24 that precipitation would have had to double for statistically significant changes in deposit thickness to  
25 be generated. We discuss how climatic signals may be lost due to the self-organization, spatial-temporal  
26 varied response and preservation potential in large fluvial systems. This study gives a new quantified  
27 perspective to climate events in the geologic record.

## 28 **INTRODUCTION**

29 Earth's present-day climate is undergoing anthropogenically induced warming, with increased  
30 temperatures and storm intensities, sea-level rises, and aridification observed and predicted across the  
31 globe (IPCC 2021, 2022). Understanding how rivers and their associated floodplains respond to climate  
32 change is critical because these environments are important biogeochemical interfaces, habitats for  
33 wildlife, conduits for delivering sediment and water to the world's oceans, as well as being areas for  
34 cultivation and habitation for humans. Climate unequivocally influences the nature of river channels and  
35 their associated floodplains. Climate provides a first-order control on the amount of water present in a  
36 fluvial system as well as influencing discharge regimes (e.g., perennial, seasonal, intermittent, and  
37 ephemeral). In addition, climate influences the rate of soil development, the type and density of  
38 vegetation present on channel bars and banks and in floodplain environments, which in turn directly  
39 impacts the caliber and sediment load present in a fluvial system by influencing, in conjunction with  
40 local geology, the erodibility of the landscape and thus sediment supply into a river system. In addition,  
41 other factors, such as slope (ultimately controlled by tectonics) and base level (e.g., sea level/lake level)  
42 will contribute towards defining the dimensions, morphology (e.g., braided, meandering, anastomosing,  
43 and straight as end members), and sediment load of a fluvial system.

44 If all factors are kept in a steady state, a river will inherently adjust to reach equilibrium (i.e., the graded  
45 profile; Mackin, 1948). However, alluvial systems that are not undergoing transient response, for  
46 example to base-level fall, are more likely to exist in a state of dynamic equilibrium with forcing  
47 conditions that themselves are constantly changing (e.g., Bull, 1991; Dade and Friend, 1998; Whipple,  
48 2001; Blum, 2008; Macklin et al. 2012). Defining dynamic equilibrium may also be problematic due to  
49 the multitude of autocyclic and allocyclic factors involved, which operate at different timescales and  
50 have differing response rates dependent on fluvial-system size, and the tendency of fluvial system to act  
51 in a hierarchal manner (i.e., different scales of the system responding to different magnitudes of change  
52 at different rates). Disentangling this complex range of interlinked factors that operate at different time  
53 scales is challenging, particularly because timescales far exceed the length of human observation (Toby  
54 et al., 2022). However, with careful observations and consideration of all factors involved, deductions  
55 can be made as to how, and why, rivers respond to different external forcing mechanisms. A change in  
56 climate will affect river discharge and sediment load through changes in precipitation, weathering, and  
57 vegetation dynamics. Changes in hydrological forcing cause fluvial morphological responses, including  
58 changes in channel and bar dimensions and migration rates, planform, bed sediment size, and net  
59 sediment flux, leading to aggradation (storage) or degradation (removal) (e.g., Bull, 1991; Knighton  
60 1998; Blum and Törnqvist 2000; Macklin et al. 2012). The timescales of these adjustments to new  
61 climatic conditions depend on the magnitude and rate of changes in the forcing factors and the  
62 sensitivity of the system to change (Blum, 2008). There are a multitude of examples available of  
63 fluvial response to changes in climate. For example, morphological changes in rivers in SE Australia have  
64 been linked to variations in flow regime consequent on Late Quaternary climatic changes (Nanson et al.,  
65 2003). Fluvial response to climate changes has also been documented in geologically based studies. For  
66 example, Chen et al (2018), report increased channel mobility and soil denudation due to increased

67 discharge and regional vegetation decline related to climate change during the early phase of the  
68 Paleocene-Eocene Thermal Maximum (PETM) in the Tremp-Graus Basin (Spain).

69 Sedimentary deposits provide insights into how Earth systems may respond in the future to extreme  
70 climate events (Pancost 2017). During the PETM (ca.56 Ma; Zachos et al. 2003) hyperthermal-event  
71 global temperatures increased because of high atmospheric CO<sub>2</sub> concentrations. Sea-surface  
72 temperatures rose by 5-9°C and bottom water temperatures increased by 4-5°C over approximately 8-  
73 23 ka during the onset of the PETM, remaining high for approximately 115ka, before a 42 ka recession to  
74 pre-PETM levels (Zachos et al. 2003; 2005; McInerney and Wing 2011). The PETM is an important, and  
75 one of the closest, analogues for current global temperature increases, and although rates of global  
76 temperature change during the PETM are estimated to have been slower than are predicted for the 21st  
77 Century (Wing and Currano, 2013), the PETM provides longer term (pre-event, event, and post-event)  
78 insights into landscape response to a rapid climate change event. Although it is noted that caution must  
79 be used when studying the deposits of deep time due to preservation bias and the stratigraphic  
80 completeness of deposits (Sadler 1981; Straub et al. 2020, Toby et al., 2022), such deposits can, and do,  
81 provide important insights into landscape response to climate-change events that cannot be observed  
82 over human timescales.

83 The Bighorn Basin is one of the most intensively studied terrestrial PETM localities globally (e.g.,  
84 Gingerich 2003; Kraus and Riggins 2007; Rose et al. 2012; Bowen et al. 2014; Foreman, 2014; Kraus et al.  
85 2015). To date, however, PETM deposits of the Bighorn Basin have not been placed into a wider  
86 stratigraphic, depositional systems context. For example, studies have concentrated on understanding  
87 successions in a single outcrop belt (e.g., Kraus et al., 2015), or channels have been compared with those  
88 that lie immediately above or below the PETM climate event in a specific study area of the basin (e.g.  
89 Foreman, 2014). In addition, it is important to understand whether there are any spatial variations in

90 recorded response to the PETM as a result of differences in location within the Bighorn Basin. As a  
91 result, the full extent of any recorded changes have not been fully evaluated in this well-studied  
92 sedimentary basin. Here we analyze the response of fluvial systems to the PETM in the Bighorn Basin  
93 through comparison of channel properties and associated deposits before, during, and after the PETM at  
94 several localities across the basin to understand 1) how different are the PETM deposits from the  
95 surrounding, wider, Paleogene stratigraphy and 2) whether there is a difference in recorded response to  
96 the event based on spatial location in a sedimentary basin. We hypothesize that, given the magnitude of  
97 reported changes in climate during the PETM, the channel deposits from within the PETM interval  
98 should be different from those both pre- and post PETM

## 99 **REGIONAL SETTING AND PREVIOUS WORK**

100 The Bighorn Basin is situated in northwestern Wyoming and south central Montana (USA) and is  
101 bounded by a number of thrust-related Laramide-age basement-cored mountain belts. These were  
102 present in the Paleogene and are still present today; namely the Beartooth Mountains to the west, the  
103 Owl Creek Mountains to the south, and the Bighorn Mountains to the east (Fig. 1). These mountain belts  
104 formed due to the breakup of the Sevier foreland basin as the tectonic regime switched from thin-  
105 skinned deformation in the Late Jurassic-Paleogene to thick-skinned deformation in the Late Cretaceous  
106 to Eocene (Snyder et al. 1976; Dickinson et al., 1988; DeCelles, 2004; Fan and Carrapa, 2014). The  
107 present-day southwestern margin of the basin is defined by the Absaroka Mountains, which are  
108 composed of the Absaroka Volcanics which formed during the mid to late Eocene and now cover early  
109 Paleocene structures (Rouse 1937; Sundell 1990). To the north, the Nye Bowler Lineament and Pryor  
110 Mountains are present but are not interpreted to have been a topographic barrier enclosing the basin  
111 (Dickinson et al.1988; Seeland 1998).

112 The Paleocene Fort Union Formation and the Eocene Willwood Formation form the Paleogene fill of the  
113 Bighorn Basin (Fig. 1), which comprise deposits of alluvial-fan, fluvial-channel, floodplain, and minor  
114 lacustrine environments (e.g. Van Houten 1944; Kraus 1985; Bown and Kraus 1987; DeCelles et al. 1991;  
115 Willis and Behrensmeyer 1995; Yuretich 1984; Kraus and Wells 1999; Owen et al. 2017, 2019). Generally,  
116 within the basin there is a gradual change from dominantly gray paleosols in the Fort Union Fm to red  
117 paleosols in the Willwood Fm, interpreted to record a change from predominantly humid to drier  
118 conditions (Willis and Behrensmeyer 1995; Kraus et al. 2007; Kraus et al. 2015). In a basin-wide  
119 sedimentological study of the Fort Union and Willwood formations by Owen et al. (2017), a facies  
120 analysis conducted (Table 2). They identified two main facies associations (channel and floodplain) with  
121 several sub-facies associations present. In the channel-facies association, four sub-facies associations  
122 were defined, namely gravelly braided stream, heterolithic dominantly braided, heterolithic dominantly  
123 meandering, and fine-grained channel fill. In the floodplain facies association minor lacustrine, paleosols  
124 (well-drained and poorly-drained), splay, and sheetflood sub-facies associations were identified. A  
125 variety of statistical information was extracted from sedimentary-log data by Owen et al. (2019),  
126 including channel presence (expressed as a percentage within each log), weighted mean grain size for  
127 the channel, average and maximum channel thickness, and story thickness. These properties were  
128 mapped across the basin, allowing a detailed paleogeographic model of the basin to be developed.  
129 Owen et al. (2019) defined four broad, laterally sourced drainage systems, namely the Beartooth in the  
130 northwest, the Absaroka to the west, the Washakie in the southwest, and the Owl Creek to the south.  
131 All of these systems fed into an unconfined axial trunk system that flowed from south to north and was  
132 approximately 150 km in length (Fig. 1). Welch et al. (2022) have corroborated this paleogeographic  
133 model through provenance analysis and have provided further insights into the westerly source of the  
134 Absaroka fluvial systems.

135 A variety of studies using several different proxies (e.g., leaf-margin analysis,  $\delta^{18}\text{O}$  analysis of mammal  
136 teeth, analyses of pedogenic carbonate nodules) have established that the PETM in the Bighorn Basin  
137 saw increased mean annual temperature and decreased precipitation, as well as changes in vegetation  
138 type, vegetation density, and mammalian fauna (Table 1). Mean annual temperature (MAT) increased  
139 during the PETM from pre-PETM values of  $15.7 \pm 2.4$  °C by 5°C, and then returned to pre-PETM  
140 conditions during the recovery phase of the event (e.g., Fricke et al. 1998; Wing et al. 2005; Snell et al.  
141 2013). Mean annual precipitation (MAP) during the PETM decreased from pre-PETM values of 1200-  
142 1300 mm year<sup>-1</sup> by 30-40% before returning to close to prior conditions (1200 mm year<sup>-1</sup>) after the  
143 PETM (e.g., Wing et al. 2005; Kraus and Riggins 2007; Kraus et al. 2013). Before the PETM, the landscape  
144 was dominantly forested with deciduous, evergreen, broad-leaved, and coniferous taxa. During the  
145 PETM a less dense dry tropical forest structure dominated by the bean family was present, but  
146 interestingly the plant communities returned to their previous configuration during the later stages of  
147 the PETM (Wing et al. 2005, Smith et al. 2008). In addition, dwarfing of mammalian fauna has also been  
148 recorded during the PETM (Gingerich 2003). It has been suggested that enhanced seasonality in rainfall  
149 (see Foreman, 2014) and temperature (Snell et al. 2013) occurred during the PETM.

150 Here we examine three outcrop belts that cover the PETM in the Bighorn Basin, two (Saddle Mountain,  
151 SM; Polecat Bench, PCB) are found within the axial system, whilst Sand Creek Divide (SCD) occurs within  
152 a small distributive system that drains from the Owl Creek Mountains (Fig. 1). Previous studies at PCB  
153 report that the paleosols become more welded (amalgamated; see Ruhe and Olson 1980) and are  
154 therefore thicker during the PETM when compared to immediately underlying pre-PETM and overlying  
155 post-PETM deposits (Kraus et al. 2015). foreman (2014) notes at SM, located in the center of the axial  
156 system (Fig 1), the presence of an uncharacteristically thick amalgamated fluvial deposit ("boundary  
157 sandstone") within the PETM interval, with gray to red/orange paleosols located both above and below  
158 the deposit. At Sand Creek Divide (SCD), a similar situation to that at PCB is reported whereby a change



159 to drier, thicker and more mature soils is observed during the PETM interval (Kraus and Riggins 2007;  
160 Rose et al. 2012).

161 Work has focused on deposits that are at, or close to, the PETM boundary at these three locations. Here  
162 we present sedimentary-log data from an additional 25 sections from across the basin (see Fig. 1), giving  
163 in total 12 sections from the Fort Union Formation and 16 from the Willwood Formation, together  
164 allowing the deposits from the three previously studied PETM locations (Fig. 1) to be placed into a wider  
165 basin context. Observations and comparisons are conducted spatially at the outcrop-belt scale and at  
166 the basin scale, as well as temporally, by statistically comparing data from the PETM to the wider  
167 Paleogene fill within a newly defined paleogeographic depositional system context (Owen et al. 2019).  
168 This approach allows the PETM sections to be considered within a basin-scale, depositional-system  
169 context, therefore allowing full assessment of fluvial response to a hyperthermal event, including an  
170 evaluation of the degree of variability in the response at a range of scales (e.g., outcrop to basin scale).

## 171 **METHODS**

172 This paper builds on the work of Owen et al. (2019) but differs by focusing specifically on the  
173 sedimentological characteristics of floodplain and channel deposits pre-, during, and post- PETM.  
174 Sedimentary-log data were collected at 50 mm resolution at 28 locations across the basin (Fig. 1),  
175 totaling 4,192 m of stratigraphy (see Appendix 1 for sedimentary log-data). Facies association and  
176 channel-body geometries were defined from sedimentary and architectural data based on the scheme  
177 of Owen et al. (2017; see Table 2). Here, a channel body is defined as being the three-dimensional form  
178 that is deposited from processes operative within channels (see Gibling 2006 for discussion). A channel  
179 body is encompassed by floodplain deposits and may be a single story or may comprise complex  
180 amalgamated deposits. Channel bodies have in previous studies been used to infer a fluvial stratigraphic  
181 response to the PETM (e.g. Schmitz and Pujalte, 2003;oreman 2014;; Chen et al. 2018). By studying

182 channel-body characteristics, insights into controlling variables (e.g., accommodation versus sediment  
183 supply linked to climate and tectonics, migration rate, planform, and deposition/erosion rates; Bridge  
184 1993) can be gained. We define a story surface as being the “*erosional elements of the active portion of*  
185 *a channel base, which incise into previous channel deposits*” sensu Owen et al. (2017). By measuring the  
186 story thicknesses, we are able to understand how incision rates, which relate directly to channel depth  
187 and discharge, vary throughout the basin.

188 The thickness of channel bodies was measured vertically where exposure permitted. Channel-body  
189 widths and story widths were not measured, as larger channel deposits commonly extend beyond the  
190 area of outcrop exposure and provide only a minimum estimate, and smaller channel bodies often lack  
191 complete exposure and equally would not provide an accurate value. Story surfaces often crosscut one  
192 another and thus do not fully represent the true widths of the channel. As a result, and to provide a  
193 consistent method for comparison, we utilize only thickness data in this study. This dataset was analyzed  
194 in its entirety where pre-PETM, PETM, and post-PETM channel data were compared. Data from the axial  
195 system alone were then analyzed separately to compare pre-PETM, PETM, and post-PETM) deposits  
196 from the same system. Data from exposures in a transect across the axial system, perpendicular to flow,  
197 were then used to understand lateral variation at approximately the same position downstream in a  
198 single system (pre-PETM, PETM, and post-PETM); see Fig. 1 for locations.

199 Where data were available, a mammalian age group was assigned (Paleocene, undiff; Tiffanian;  
200 Clarkforkian; Wasatchian-1 to Wasatchian-4; Wasatchian-5 to Wasatchian-7) to each of the sedimentary  
201 logs based on the work of Gingerich and Clyde (2001), allowing an approximate biostratigraphic  
202 framework to be established for the sedimentary logs. Isotopic curves that indicate the start of the  
203 PETM and sedimentary log data were utilized from previously published datasets (Kraus and Riggins  
204 2007; Foreman 2014; Kraus et al. 2015) to pinpoint the location of the PETM.

205

## RESULTS

206

### *SEDIMENTARY OBSERVATIONS OF PETM SECTIONS*

207 Sedimentary logs and example images for the three studied PETM outcrop belts in the Bighorn Basin,  
208 shown in Figures 2, 3, and 4, show considerable differences. At Sand Creek Divide (isotopic data utilized  
209 from Rose et al., 2012) the pre-PETM section is dominated by drab gray soils and minor channel units  
210 (Fig. 2, 3A). In the Pre-PETM succession paleosols are gray, with orange to purple mottling present. They  
211 are generally moderately to well developed and rich in organic matter with leaf beds present.

212 Interspersed between the paleosols are small-scale (up to 8 m thick) single-story channel deposits that  
213 display trough cross-bedding and accretion surfaces. Towards the top of the pre-PETM succession (base  
214 of SD-d.2 and SD-e.1; Fig. 2, 3A, B) a gradual change in the color of the soils is observed from orange to  
215 red. The red soils, which are moderate to well-formed, then start to dominate the succession during the  
216 PETM and continue to dominate in the post-PETM succession (SD-e.1; Fig. 2,3B). No channel deposits  
217 were recorded in the PETM interval at SCD. A series of logs lateral to the main PETM section (SD-e.1; Fig.  
218 2) were measured (using isotopic data and “Red 1” of Rose et al. 2012 as a marker bed with beds being  
219 laterally traced). In log SD-e.1, the onset of the PETM shows a gradual transition in the occurrence and  
220 maturity of the red soils. SD-d.2, however, does not show any indication of a change in the nature of the  
221 soils at the start of the PETM and continues to be dominated by gray soils with purple and orange  
222 mottling present well into the PETM (Fig. 2). Interestingly, farther up the vertical section, lateral changes  
223 are also visible. At the onset of the PETM recovery, SD-e1 shows a thick, very mature paleosol (“big red”;  
224 Fig 2. 3B), However, laterally this soil is considerably thinner (SD-e.2) but still forms a mature soil  
225 dominated by red and purple mottling. In addition, in SCD1, a thick (10 m), multistory channel is  
226 observed lateral to and slightly above, ‘big red’ (i.e. the bed above; logSD-f-Fig 2) whereas laterally (SD-  
227 e.2) floodplain deposits dominate, with only moderate gray paleosol development indicating wetter

228 conditions. Therefore, a large degree of variability is present in the PETM deposits in the SCD outcrop  
229 belt. Similar observations have been made by Kraus and Riggins (2007) in the same outcrop belt, noting  
230 a change to more welded (amalgamated), thicker and drier soils during the PETM, but that the red well-  
231 drained B horizon vertic paleosols do grade laterally into poorly drained gray paleosols that are  
232 interpreted to be Bssg horizons of Vertisols.

233 At Polecat Bench only a small part of the pre-PETM succession is exposed and the succession is  
234 dominated by gray, poorly formed paleosols with orange mottling (Fig. 4A). However, close to the PETM  
235 onset (approximately 8.5 m PCB log; Fig. 4A) well-developed red soils begin to gradually appear and then  
236 dominate the lower part of the PETM succession. From ~25 m in the section and upwards, channel  
237 deposits appear within the PETM succession. Channel deposits in the PETM are dominated by lower-  
238 flow-regime structures such as trough cross-bedding and ripples, which are composed only of  
239 moderately sorted sandstone with very coarse sand to granule-grade material present on some cross-  
240 sets. The channel deposits become thicker and more frequent up-section, but, the exact location of the  
241 recovery period is inferred at this specific location due to channel erosion, with the final channel deposit  
242 proposed to be above the PETM interval (Gingerich 2001). In between the channel deposits the  
243 paleosols continue to be red, mature, and well-formed with carbonate nodules, mottling, and root  
244 structures present. Other studies at the Polecat Bench outcrop belt have noted similar trends where a  
245 change to more welded, thicker and drier soils is observed during the PETM (Kraus et al. 2015). In  
246 addition, a sedimentary log has been constructed from a core that was retrieved from behind ( (approximately  
247 100m) the outcrop exposure (Fig. 2 of Kraus et al. 2015). The authors noted in the core, a  
248 change to more mature, more welded soils is observed during the PETM succession, and that channel  
249 and related splay deposits are more abundant in the core compared to sedimentary logs taken at the  
250 outcrop. We observe similar channel and related splay deposits in our sedimentary log (e.g.,  
251 approximately 35 m, Fig. 4A). Thus, although similarities can be observed between the three logs, such

252 as the dominance of red mature paleosols over other types of paleosols, there is inherent variability in  
253 the presence of channel deposits in the PETM interval at the Polecat Bench outcrop belt. A key  
254 difference between our logs and those previously published, however, is that we observe one relatively  
255 thick (4 m) channel in our log (~=approximately 26 m, Fig. 4A).

256 A noticeable change in the nature of the PETM succession is observed at the Saddle Mountain outcrop  
257 belt, which is situated in the middle of the basin in the axial system. The base of the recorded succession  
258 (below the PETM) is dominated by a 17-m-thick multistory (three stories) channel body with lower-flow-  
259 regime structures present (trough cross-bedding and ripples) (Fig. 3C, 4B). The succession above this is  
260 then dominated by floodplain deposits which are composed predominantly of gray soils with orange and  
261 purple mottling that become increasingly redder towards the top of the pre-PETM succession. In the  
262 PETM interval the base is dominated by floodplain deposits composed of red paleosols and splay  
263 deposits; however, a large, internally amalgamated channel body appears from approximately 60-84 m  
264 on the log. The channel body is thick (24 m), is composed of four stories with accretion surfaces, with  
265 trough cross-bedding and planar to low-angle planar lamination present (Fig. 3). Wood debris, carbonate  
266 nodules, and coarser grained material commonly line cross sets. Separating the stories are thin (up to 4  
267 m) packages of green to gray mud and fine sandstone sheets within which carbonate nodules, woody  
268 debris and plant material can be observed. Above the channel body a thick (9 m) floodplain package is  
269 present which is dominantly gray and contains one mature red paleosol with rootlets and carbonate  
270 nodules present. An additional channel body was observed in the outcrop during the PETM recovery  
271 onset that is thinner (10 m) than the channel observed in the PETM proper but is very similar  
272 sedimentologically. However, this channel body has a slightly different geometry in that it has an offset  
273 stacked pattern (Fig.4). Foreman (2014) also documented the presence of a large channel body (the  
274 "boundary sandstone") within the PETM interval. He noted that the boundary sandstone varies in  
275 thickness across the outcrop belt as well as displaying variations in stacking arrangement and the

276 presence of mud in the channel body and between story surfaces. These observations, again, highlight  
277 the variability observed in PETM successions in single outcrop belts.

278 In summary, the field observations from each of the three outcrop belts highlight that there is a  
279 considerable variability in fluvial facies characteristics both in single outcrop belts and between the  
280 different outcrop belts across the basin when looking at deposits within, and immediately above, and,  
281 below the PETM. These observations raise the question as to whether it is possible to identify a  
282 consistent, contemporaneous environmental change within the PETM across the basin given the  
283 variations observed in each of the logged sections, given the magnitude of change in precipitation and  
284 temperatures that has been reported to occur in the basin.

#### 285 *STATISTICAL ANALYSIS*

286 To assess the impact of climate change on the fluvial system, PETM channel bodies (N = 3) are compared  
287 with those from the pre- (n = 109) and post-(n=73) PETM successions. This small sample size for PETM  
288 channels reflects the paucity of channel bodies in this part of the basin rather than sampling bias (see  
289 Appendix for logs of entire basin and Paleogeography of Owen et al. 2019), particularly in documented  
290 PETM intervals. However, whilst this is a small sample size, it is compared to much larger datasets from  
291 the pre- and post-PETM stratigraphy. The mean channel-body thickness of the PETM channel bodies  
292 ( $12.40 \pm 5.9$  m;  $cv = (\text{standard deviation}/\text{mean}) = 0.82$ ; N = 3) exceeds both pre- ( $7.49 \pm 0.69$  m;  $cv =$   
293  $0.96$ ; N = 109) and post- ( $7.66 \pm 0.78$  m;  $cv = 0.87$ ; N=73) PETM values for the whole basin. When  
294 considering just the axial system (where PETM channel bodies are found), the pre-PETM average  
295 thickness ( $7.65 \pm 0.77$  m;  $cv = 0.53$ , N = 28) and post-PETM average thickness ( $7.19 \pm 0.64$ m;  $cv = 0.49$ ; N  
296 = 30) are both smaller than PETM values ( $12.40 \pm 5.9$  m;  $cv = 0.82$ ; N = 3). When considering just a  
297 transect through the northern part of the axial system (i.e., channel deposits at the same position

298 downstream in the axial system) PETM channel bodies are on average larger than those pre-PETM ( $7.75$   
299  $\pm 0.88$  m;  $cv = 0.56$ ;  $N = 24$ ) and post- ( $8.25 \pm 0.93$  m;  $cv = 0.39$ ;  $N = 12$ ) PETM.

300 The coefficients of variation for the whole-basin dataset are greater than for the whole axial (pre-PETM  
301  $0.53$ ; post-PETM  $0.49$ ) and northern axial (pre-PETM  $0.56$ ; post-PETM  $0.39$ ) transects. None of the  
302 differences above (whole basin, Northern axial, axial) in mean channel-body thickness (pre-, during, and  
303 post-PETM) are statistically significant (ANOVA;  $p$ -values =  $0.33$  whole basin data (log transformed);  
304  $0.27$  Northern axial,  $0.13$  axial).

305 PETM channel-body thicknesses lie within the range of measured channels from the Paleogene fill (Fig.  
306 5A), with the average PETM measurement falling within the range (mean  $\pm 1$  standard deviation) of all  
307 datasets analyzed. Indeed, the measured channel thicknesses for the PETM are not the largest in the  
308 basin (Fig. 6), with channel measurements from Foreman (2014) for the PETM also lying within the  
309 range of measured channel body thicknesses in our basin-wide dataset.

310 However, the story (channel depth) thickness dataset shows different results. The mean story thickness  
311 of the PETM channel bodies ( $4.65 \pm 0.98$  m;  $cv = 0.59$ ;  $N = 8$ ) is very similar to the pre-PETM ( $4.67 \pm 0.27$   
312 m;  $cv = 0.73$ ;  $N = 154$ ) and post-PETM ( $4.67 \pm 0.22$  m;  $cv = 0.47$ ;  $N = 101$ ) values for the whole basin.

313 When considering just the axial system, the pre-PETM average story thickness ( $4.29 \pm 0.24$  m;  $cv = 0.39$ ,  
314  $N = 50$ ) and post-PETM average thickness ( $4.49 \pm 0.29$  m;  $cv = 0.44$ ;  $N = 48$ ) are only slightly smaller than  
315 PETM values ( $4.65 \pm 0.98$  m;  $cv = 0.59$ ;  $N = 8$ ). For the northern transect across the axial system (See Fig.  
316 1 for location) PETM channels are again only slightly larger than pre-PETM ( $4.54 \pm 0.27$  m;  $cv = 0.38$ ;  $N =$   
317  $41$ ) and post-PETM ( $4.30 \pm 0.31$  m;  $cv = 0.35$ ;  $N = 23$ ) values.

318 Story thicknesses for the PETM interval are within the range of all other datasets (e.g., pre- and post-  
319 PETM) Fig. 5B) with the exception of the post-PETM northern transect dataset where the range in story

320 thicknesses is smaller. However, the average story thickness of the post-PETM northern transect still lies  
321 within the range of measured story thicknesses for this dataset. In all but the pre-PETM basin-wide  
322 dataset, the coefficient of variation is larger for PETM deposits than either pre- or post-PETM deposits,  
323 which is to be expected due to the smaller sample size for the PETM. The lack of any significant change  
324 in channel depth indicated by the story thickness suggests that the axial fluvial system did not undergo  
325 significant change in morphology or size through the PETM period. The channel body data support this;  
326 although the three PETM channel bodies are on average thicker than both pre- and post PETM, this is  
327 not a statistically significant difference. As was the case for the channel-body deposits, none of the  
328 differences in mean story thickness (pre-, during, and post-PETM) are statistically significant (ANOVA; p-  
329 values = 0.48 whole basin data (log transformed); 0.85 Northern axial; 0.81 axial).

## 330 **DISCUSSION**

### 331 *EXPECTED STRATIGRAPHIC RESPONSE TO CLIMATE CHANGE*

332 The analysis of measured channel-body and story thicknesses shows significant variability within each  
333 time interval and, although mean values do show some differences within the PETM, these are not  
334 statistically significant given the high degree of observed variability. To further assess the significance of  
335 these results, we consider the potential stratigraphic response of the Bighorn Basin axial fluvial system  
336 to the PETM by calculating expected channel size based on the 30% reduction in precipitation that has  
337 been estimated to occur from pre-PETM to the PETM (e.g. Wing et al. 2005; Kraus and Riggins 2007;  
338 Kraus et al. 2013) (Table 4). However, this reduction in mean precipitation is likely to have been  
339 accompanied by increased seasonality such that formative discharge events may have increased in  
340 magnitude during the PETM (Foreman, 2014) so causing increase in story thickness. The statistical  
341 analysis is restricted to the axial system to avoid bias imparted by the different size lateral systems  
342 present along the basin margins. Using values for the mean, standard deviation and sample size (N)



343 reported above, we calculate the increase in mean story thickness required during the PETM for this to  
344 be statistically significant (using a t-test to compare pre-PETM and PETM values). Note that the small (N  
345 = 8) number of PETM values leads to a relatively high standard deviation for this interval, which results  
346 in high story-thickness increases being required in order to be statistically significant. To account for the  
347 sample-size effect on estimated standard deviation, a further calculation was made using the lower pre-  
348 PETM standard deviations as an indication of natural variability in the deposits. This approach suggests  
349 conservative (lower) increases in thickness necessary to be statistically significant.

350 To represent a statistically significant increase, the minimum PETM average story thickness in the  
351 northern axial transect would be 5.80 m (Table 4), (+ 1.27 m pre-PETM mean and +1.15 m higher than  
352 the PETM mean). The significant story thickness rises to 6.46 m using the standard deviation from the  
353 eight PETM measurements. For the whole axial system, the significant mean thickness would be 5.49 m  
354 (+1.21 m of pre-PETM and +0.85 m than PETM mean; Table 4). Again, using the measured standard  
355 deviation estimate increases the significant mean value, here to 6.19 m.

356 The statistically significant changes in channel depth (story thickness) can be used to estimate the  
357 increase in discharge ( $Q$ ) that would be required to produce channel adjustments of this magnitude. We  
358 used a hydraulic-geometry relationship (Leopold and Maddock, 1953)

$$359 \quad h = cQ^f$$

360 where  $h$  is flow depth [m], and  $c$  and  $f$  are empirical constants. The exponent  $f$  is taken as 0.4, based on  
361 extensive global data (Knighton, 1998). To generate statistically significant depth changes for a single  
362 channel located along the northern axial transect,  $Q$  needs to increase by a factor of 2.42 using story  
363 thickness calculated with the standard deviation from the PETM data (N = 8) (Table 2). For the axial  
364 system dataset a similar magnitude of increase is suggested (2.51; Table 2). These results show that a

365 statistically significant stratigraphic response requires increased discharge, and therefore storm-event  
366 runoff (Knighton 1998) during the PETM to more than double compared to pre-PETM values. Such an  
367 increase in discharge, which could be related to increased storm-event precipitation and runoff from  
368 sparsely vegetated hillslopes, is opposite to estimates (30% decrease) of mean annual precipitation  
369 changes from pre-PETM to the PETM (Table 1).

370 Increasing seasonality of precipitation and river discharge could lead to channel-geometry adjustments  
371 (Knighton 1998), and more variable flow will also affect the nature of deposits (e.g., Fielding et al. 2009;  
372 Plink-Björklund 2015). Potentially enhanced seasonality in rainfall (Foreman, 2014) and temperature  
373 (Snell et al. 2013) during the PETM could have resulted in increased storm-event precipitation while  
374 overall precipitation decreased. However, recent modelling indicates complex atmospheric behavior in  
375 the Bighorn Basin and suggests a reduction in extreme precipitation rates, although when high CO<sub>2</sub>  
376 levels are modelled an increase in the rarest precipitation events may have occurred more often  
377 (Carmichael et al. 2018). Carmichael et al. (2018) note that although these inferred responses are  
378 contradictory, precipitation events in the area are broadly regular and of low intensity. Grain-size  
379 datasets for channels (Owen et al. 2019) show that the PETM channel sediments (average 0.27 mm) lie  
380 in the range of those within the northern axial transect (average 0.21 - 0.47 mm) implying no significant  
381 change in river bed sediment size during the PETM. Story surface depths do not change significantly, and  
382 there is little change in the sedimentology of the channels, with bedforms remaining similar to those in  
383 both pre- and post-PETM deposits (Foreman, 2014). The internal sedimentology of the fluvial channels  
384 therefore suggests that enhanced seasonality, if present, had little effect on the resultant preserved  
385 channel-deposit characteristics. This is not wholly surprising given the axial river location as most of the  
386 coarsest material is trapped upstream in the proximal part of the basin, in basin-margin-transverse  
387 systems.

389 A change in climate, causing changes in river discharge and sediment loads, will result in geomorphic  
390 and sedimentological changes, the magnitude of which will depend on the nature of the river system  
391 and its sensitivity to change. Thus, fluvial sediments deposited during a climate event may be different  
392 from those before the event. For the environmental changes that resulted from the PETM in the Bighorn  
393 Basin to be recorded in the three studied PETM outcrop belts, the response of the fluvial system to  
394 these changes would need to be propagated from the source catchments through multiple transverse  
395 systems that supplied the axial system in the basin. Regionally, river systems can respond synchronously  
396 to climatic changes (e.g., Bull 1991; Macklin et al. 2002), but more frequently they respond at different  
397 rates and times (e.g., Starkel 1991; Slater and Singer 2013). Whether responses are regionally consistent  
398 depends on the magnitude and rate of forcing, with larger, faster changes in environmental conditions  
399 being more likely to result in synchronous and consistent responses. If all catchments in the Bighorn  
400 Basin responded synchronously to the PETM, the signal in the axial system should be amplified.  
401 However, if the lateral systems responded at different times and rates, a dampened and extended signal  
402 of the climate event would be expected in the axial system. The latter scenario is expected because the  
403 lateral river systems are of differing sizes and will respond at different rates to external perturbations  
404 (Blum 2008). Hence a muted signal is hypothesized to reach the distal reaches (e.g. Saddle Mountain,  
405 Fig. 1) of the axial system. Numerical models demonstrate that rivers can attenuate or absorb external  
406 signals through internal system dynamics (e.g., avulsion, sediment storage and release), and suggest  
407 that significant geomorphic thresholds (e.g., critical slope; Schumm 1979) need to be met for  
408 environmental signals to be recorded (e.g., Jerolmack and Paola 2010; Straub et al. 2020). Indeed,  
409 recent work by Ganti et al. (2020) using theoretical and field-based studies suggests that the  
410 stratigraphic record captures ordinary events ("*Strange ordinarieness*", Paola et al. 2018) due to the  
411 inherent manner in which fluvial systems self-organize. Ganti et al. (2020) showed from modelling that

412 higher sedimentation rates should lead to higher preservation potential of bar deposits during the PETM  
413 (compared to pre- and post-PETM); however, if higher sedimentation rates led to increased avulsion and  
414 migration rates, then preservation of extreme conditions would be consistent across pre-PETM, PETM,  
415 and post-PETM strata. Our sedimentological observations (e.g., grain size, cross-set height, and story  
416 height) from strata during and across the Paleocene and Eocene support the latter conclusions drawn by  
417 Ganti et al. (2020). These combined factors result in a low likelihood of a short-term signal being  
418 preserved within the geologic record.

419 A more amalgamated body (“boundary sandstone”) is present at Saddle Mountain during the PETM  
420 (Figs. 3C, Fig 4; Foreman, 2014); however, the boundary sandstone is not consistently thick (Foreman,  
421 2014) nor is it anomalous with respect to its stacking geometry when compared to other sandbodies in  
422 this area (i.e., axial fluvial system, northern transect) of the basin (e.g., Fig.7B; Owen et al. 2017). It is  
423 argued by Foreman (2014) that the boundary sandstone resulted either from deposition induced by  
424 adjustment of river gradient to changes in supply of sediment and water, or from decreased bank  
425 stability due to a decrease in vegetation cover. Modelling of the former (Simpson and Castelltort 2012)  
426 shows that a significant distal response is expected only once wetter conditions with higher transport  
427 capacities return. Hence, because of the inference of a decrease in mean annual precipitation during the  
428 PETM (Table 1), any change in channel form should be observed either in the later PETM or early post-  
429 PETM deposits after a return to pre-PETM precipitation values, particularly because a lag time of 14-25  
430 ky is to be expected in the Bighorn Basin (Duller et al. 2019). Our data do not support the alternative  
431 scenario of decreased bank stability, inasmuch as a shallowing and change in planform are not observed,  
432 which would be expected if bank stability decreased as rivers would widen. In addition, other published  
433 PETM sedimentary logs show that more welded and/or amalgamated soils can be present (although  
434 laterally variable) such as those seen at Polecat Bench (Kraus et al. 2015), implying that a more  
435 structured and cohesive floodplain was present, which would in turn result in an increase in bank

436 stability. Given the boundary sandstones variable thickness in the depocenter of the basin, we  
437 hypothesize that autogenic processes such as avulsion have driven the formation of a larger sandstone  
438 body at SM where the axial system is present. A thicker sand body may therefore be a local expression  
439 of internal system dynamics rather than indicating a response to external drivers (Jones and Hajek  
440 2007).

441 The preservation of autocyclic processes over allocyclic processes in the stratigraphy of the Bighorn  
442 Basin fluvial systems is not unexpected when considering the paleogeography of the basin. The fluvial  
443 systems that entered the Bighorn Basin were supplied from different catchments of variable sizes (Fig. 1;  
444 Owen et al. 2019). The Absaroka and Washakie catchments fed and resulted in large, coarse-grained  
445 fluvial systems sourced from outside the immediate basin area. In contrast, the Beartooth and Bighorn  
446 mountains are considered to have been source areas for locally derived alluvial and fluvial fans, with the  
447 Owl Creek catchment to the south supplying relatively small-scale fluvial systems to the basinal area  
448 (Owen et al. 2019). Of the studied sections, Sand Creek Divide was supplied solely from the Owl Creek  
449 catchment, whereas Polecat Bench and Saddle Mountain are both located within the axial fluvial system  
450 (Fig. 1). Thus, Sand Creek Divide will record only a climatic response from the Owl Creek drainage,  
451 whereas Saddle Mountain and Polecat Bench will record an amalgamation of climate responses from  
452 immediately adjacent alluvial and fluvial fans, the Owl Creek, Washakie, and Absaroka catchments. It is  
453 expected that these catchments will respond over different time scales to any climatically induced  
454 perturbation depending on elevation, gradient, size, grain-size availability, bedrock lithology, and  
455 downstream distance to the logged sections (Duller et al. 2019). Thus, any allocyclic climate signal in an  
456 axial fluvial system is likely to be shredded by a combination of different lag times in different-sized  
457 catchments as well as ongoing autocyclic processes such as avulsion. Further modelling work is needed  
458 to quantitatively explore how having multiple, and different sized, pathways in a source-to-sink system  
459 will affect the expected signal propagation and resultant stratigraphy, particularly with regard to

460 preservation in axial systems. A record of a global climate signal in a fluvial system is more likely to be  
461 preserved if the fluvial system is sourced either from a single catchment area with a uniform climate, or  
462 where immediately adjacent catchments respond to the same climate event, such as in a bajada-type  
463 setting (e.g., Cesta and Ward, 2016).

464 When analyzing the effects of climate on fluvial systems, it is imperative that other factors, such as  
465 tectonics and baselevel, have been accounted for (Vandenberghe, 2002, Macklin et al. 2012). The role of  
466 tectonics in the Bighorn Basin has largely been disregarded (Foreman 2014); however, our basin-wide  
467 study shows evidence of tectonic processes (Fig. 7A). The assumption that there was a lack of tectonic  
468 activity during the PETM cannot be made, because there are unconformities present that span the  
469 Paleocene-Eocene, providing evidence for tectonic activity around the basin margin (Fig. 7A). Thus, with  
470 syntectonic activity it is expected that subtle increases and decrease in accommodation, along with  
471 sediment-supply variations due to uplift and/or exposure, and changes in channel amalgamation rates  
472 could be another way in which thicker deposits can be formed, particularly in axial systems (e.g., Connell  
473 et al. 2012). Variable subsidence rates have been found across the basin (Clyde et al., 2007), with slow  
474 rates of subsidence in the SE (Owl Creek systems, approximately 85 m/Myr.) but high rates in other  
475 areas such as McCullough Peaks (approximately 250 m/Myr) and Polecat Bench (approximately 200  
476 m/Myr) both situated in the axial part of the basin.

477 Prior comparisons of the sedimentology of the PETM successions have been made only during the PETM  
478 and immediately before and after the PETM event (e.g., Kraus et al. 2015; Foreman 2014). Cyclicity, i.e.,  
479 repeated channel and floodplain deposition, is evident in the basin fill, and is an order of magnitude  
480 larger than the discussed study intervals for the PETM. Channel bodies have a return thickness of  
481 approximately 20-30 m in the axial system (see Fig. 7C for example), whereby the top of one channel  
482 body is separated by approximately 20-30 m of floodplain deposits before the base of the next

483 sandbody is encountered. Although the PETM spans only a single channel-body avulsion package, it is  
484 essential that the deposits are discussed within the context of the overall system dynamics, which, in the  
485 case of the Bighorn Basin, requires the study of channel-body deposits 20-30 m above and below in  
486 order for an assessment for any significant changes to be made. Our basin-scale dataset considers the  
487 gross-depositional fill of the basin by studying the deposits substantially below and above those of the  
488 PETM. In addition, mature, red paleosols are not unique to the PETM. In the basin fill, multiple mature,  
489 red paleosols are present below, but more commonly above, the PETM in both the axial (Fig. 7C) as well  
490 as the surrounding lateral systems (e.g., Kraus and Wells, 1999; Kraus, 2001; Abels et al. 2013. This  
491 implies that the paleosols are either not unique to this particular climate event and can be formed  
492 through other mechanisms (e.g., areas of the floodplain that are dry due to a position distal to a  
493 channel) or that to generate such paleosols there is a need for other climate events that have not, as  
494 yet, been identified in the basin fill.

495 We stress that we are not implying that river dynamics and deposits may not respond to climatic  
496 changes, but that the stratigraphic signature is negligible, or signal-to-noise (i.e., autocyclic processes) is  
497 too low to be detectable in the Bighorn Basin when placed into a wider stratigraphic and systems  
498 context. In much more climatically sensitive areas, a similar degree of climate change could have more  
499 significant consequences. Our results suggest that in this particular climate zone the magnitude and rate  
500 of environmental changes associated with the PETM are insufficient to overcome geomorphic  
501 thresholds controlling channel pattern and size and so are not recorded in a statistically significant way  
502 in the geological record in the axial and Owl Creek systems. We fully recognize that channel-body  
503 deposits, at the extreme end of the data, are thicker than those of similar deposits (e.g., in the axial  
504 fluvial system); however, this channel body is not uniformly thick across the axial system with the  
505 average thickness of the channel body sitting within the “norm” of channel deposits. In addition,  
506 sedimentary-log data from other localities show that there is considerable variation laterally even at the

507 outcrop-belt (several kilometers) scale, as is observed by the variable thickness of channel and splay  
508 deposits in the “boundary sandstone interval” at Polecat Bench and Saddle Mountain (Fig. 4) and the  
509 nature of paleosols deposits at Sand Creek Divide (Figs. 2, 3). Such variability is to be expected across a  
510 landscape dominated by fluvial systems as environments transition from one to another (e.g., fluvial  
511 channel to proximal to distal floodplain) with local hydrological conditions, vegetation and topography  
512 influencing characteristics at a local and basin scale. However, our study follows the principles of  
513 Walther’s Law (Middleton, 1973) and highlights that when studying the influence of events, such as  
514 climatic fluctuations on systems, it is imperative that natural landscape variability (i.e., spatial variability)  
515 is taken into consideration, as different interpretations of the effect of events may differ depending on  
516 where log locations are taken on the relict landscape. Indeed, recent work by Dzombak et al. (2021)  
517 demonstrated variability in paleosol proxy work along an extensive outcrop belt in the Green River  
518 Basin, SW Wyoming. This work highlights that there is inherent uncertainty when using proxies from  
519 single sections to infer basin-scale trends and that it is important to understand the true variability that  
520 can be present.

## 521 **CONCLUSIONS**

522 Our study provides a unique framework for analyzing climatic events in the terrestrial rock record by  
523 highlighting the importance of considering sedimentary signatures interpreted to be generated by  
524 climate change within a wider stratigraphic and depositional systems context. Our results indicate that  
525 sedimentary patterns during the PETM are not consistent across single outcrop belts in the Bighorn  
526 Basin, let alone across the entire basin, with river behavior during the PETM being within the normal  
527 range found in the rest of the basin fill. This result is not wholly unexpected given Walther’s Law, but it  
528 highlights the importance of studying climate events with appropriate contextual data. Our results  
529 suggest that the PETM climatic perturbation was not of sufficient duration or magnitude to generate a



530 statistically significant fluvial stratigraphic response in the axial or Owl Creek systems of the Bighorn  
531 Basin. Our calculations from a single channel show that a significant (more than double pre-PETM levels)  
532 increase in storm-event precipitation would be required for a clear stratigraphic response. This study  
533 has important wider implications for how we understand the spatial variability in environmental  
534 response to climate events and how we appropriately utilize the stratigraphic record to project future  
535 climatic response.

#### 536 **ACKNOWLEDGMENTS**

537 AO, AH, and GW thanks FSRG 2 sponsors for funding field campaigns. AE thanks University of Aberdeen  
538 for funding field work. We thank all residents in the Bighorn Basin who allowed access to private land to  
539 study the Paleogene fill, which greatly enhanced the size and quality of this dataset. Isobel Buchanon,  
540 Alistair Swan, and Mauricio Santos are thanked for their assistance in the field.

541

#### 542 **FIGURE CAPTIONS**

543 Figure 1 A) Paleogeography of the Bighorn Basin during the Paleogene and localities studied. Modified  
544 from Owen et al. (2019). Please see Appendix 1 for sedimentary logs of locations. B) Generalized  
545 stratigraphic column of the study area.

546 Figure 2. Sedimentary logs taken across the Sand Creek Divide outcrop belt. Location of PETM (i.e.  
547 isotopic data), "Big Red" and "Red 1" taken from Rose et al. (2012).

548 Figure 3. Example images of the PETM. A) Image of log location at SD-d1 and d2 at Sand Creek Divide.  
549 Note that this log is lateral to the image in part B. B) Image of log SD-e1. Note the persistence of red  
550 soils that laterally turn gray in part A. C) Boundary sandstone at Saddle Mountain. Note the presence of

551 mudstone packages in the boundary sandstone that clearly separate stories in the channel body. Please  
552 see Figure 4, or Appendix 1, for sedimentary log detail

553 Figure 4. A) Sedimentary logs of Polecat Bench. PETM location in the stratigraphy taken from Kraus et al.  
554 (2015). B) Sedimentary log of Saddle Mountain. PETM location in the stratigraphy is taken from Foreman  
555 (2014).

556 Figure 5. Box and whisker plots summarizing the measured data. A) Channel-body thickness and B) story  
557 thickness. In this study story surfaces are considered to represent channel depth as they scale to bar  
558 clinoform height (and therefore flow depth).

559 Figure 6. Histogram data for all channel bodies in the Bighorn Basin. Note that PETM channel-body  
560 thicknesses are highlighted with stars (this study) and those recorded in other studies (arrows).

561 Figure 7. A) Angular unconformity in the SW part of the basin. Note dipping, interbedded channel and  
562 floodplain deposits of the Fort Union (Paleocene) and flat-lying conglomeratic units of the Willwood  
563 (Eocene) deposits. B) Photopanel of axial fluvial deposits in the western area of the northern transect of  
564 the axial fluvial system. Note the occurrence of thick sandstone bodies that occur every 20-30 m in the  
565 basin fill stratigraphy. C) McCullough peaks exposure highlighting the persistence of thick red soils  
566 elsewhere in the stratigraphy.

567 **TABLE CAPTIONS**

568 Table 1. Summary of key characteristics pre-PETM, PETM, and post-PETM in the Bighorn Basin.

569 Table 2. Summary descriptions of facies associations observed in the Paleocene and Eocene fill of the  
570 Bighorn Basin (see Owen et al., 2017, for full descriptions of facies and geometries).

571 Table 3. Summary data (in meters) for channel-body and story deposits pre-PETM, PETM, and post-  
572 PETM for the whole basin, whole axial system, and northern basin transect. See Figure 5 for graphical  
573 representation of dataset.

574 Table 4 - Summary statistical results comparing pre-PETM and PETM channel depths (story thicknesses).  
575 Results are presented for two assumptions for standard deviations, s.d., for the PETM data: (1) s.d.  
576 calculated from all eight available measurements; (2) s.d. estimated as being the same as in the larger  
577 pre-PETM data sets for the same locations. The estimates of channel-forming discharge were calculated  
578 using  $f = 0.4$  in an empirical relationship between channel depth,  $h$ , and discharge,  $Q$ ,  $h = cQ^f$ .

## 579 APPENDIX

580 The appendix contains five sections, each of which shows the summarized raw sedimentary logs for all  
581 locations studies. Section A1.1: Sedimentary logs from the Beartooth systems. Section A1.2:  
582 Sedimentary logs from the Absoraka systems. Section A1.3: sedimentary logs from Washakie  
583 sedimentary systems. Section A1.4: sedimentary logs from the Owl Creek systems. Section A1.5:  
584 sedimentary logs from the Axial system.

## 585 REFERENCES

586 Abels, H.A., Kraus, M.J., and Gingerich, P.D., 2013, Precession-scale cyclicity in the fluvial lower  
587 Eocene Willwood Formation of the Bighorn Basin, Wyoming (USA): *Sedimentology*, v. 60, p.  
588 1467-1483.

589 Blum, M.D., 2008, Large River Systems and Climate Change, *in* Gupta, A. ed., Large Rivers:  
590 Geomorphology and Management: John Wiley & Sons, p. 627–659.

591 Blum, M.D., and Törnqvist, T.E., 2000, Fluvial responses to climate and sea-level change: a review and  
592 look forward: *Sedimentology*, v. 47, p. 2–48.

593 Bowen, G.J., Maibauer, B.J., Kraus, M.J., Röhl, U., Westerhold, T., Steimke, A., Gingerich, P.D., Wing,  
594 S.L., Clyde, W.C. 2014 Two massive, rapid releases of carbon during the onset of the  
595 Palaeocene-Eocene thermal maximum: *Nature Geoscience*, v. 8, p. 44-47.

596 Bown, T.M., and Kraus, M.J., 1987, Integration of channel and floodplain suites, developmental  
597 sequence and lateral relations of alluvial paleosols: *Journal of Sedimentary Petrology*, v. 57, p.  
598 587–601.

599 Bull, W.B., 1991, *Geomorphic Responses to Climate Change*: Oxford, Oxford University Press, 326.p.

600 Bridge, J.S., 1993, Description and interpretation of fluvial deposits: a critical perspective:  
601 *Sedimentology*, v. 40, p. 801–810.

602 Carmichael, M.J., Pancost, R.D., and Lunt, D.J., 2018, Changes in the occurrence of extreme  
603 precipitation events at the Paleocene–Eocene thermal maximum: *Earth and Planetary Science*  
604 *Letters*, v. 501, p. 24–36.

605 Cesta, J.M., and Ward, D.J., 2016, Timing and nature of alluvial fan development along the Chajnantor  
606 Plateau, northern Chile: *Geomorphology*, v. 273, p. 412-427.

607 Chen, C., Guerit, L., Foreman, B.Z., Hassenruck-Gudipati, H.J., Adatte, T., Honegger, L. Perret, M.,  
608 Sluijs, A., and Castelltort, S., 2018, Estimating regional flood discharge during Palaeocene-  
609 Eocene global warming: *Scientific Reports*, v. 8, P. 1-8.

610 Clyde, W.C., Hamzi, W., Wing, S.L., Schankler, D., Chew, A., 2007, Basin-wide magnetostratigraphic  
611 framework for the Bighorn Basin, Wyoming: Geological Society America Bulletin, V.119, p.  
612 848-859.

613 Connell, S.D., Wonsuck, K., Paola, C., and Smith, G.A., 2012, Fluvial morphology and sediment-flux of  
614 axial-transverse boundaries in an experimental basin: Journal of Sedimentary Research, v. 82,  
615 p. 310-325.

616 Dade, W.B., and Friend, P.F., 1998, Grain-size, sediment transport regime, and channel slope in  
617 alluvial rivers: Journal of Geology, v. 106, p. 661–675.

618 DeCelles, P.G., Gray, M.B., Ridgway, K.D., Cole, R.B., Srivastava, P.N., and Pivnik, D.A., 1991, Kinematic history of  
619 a foreland uplift from Paleocene synorogenic conglomerate, Beartooth Range , Wyoming and Montana:  
620 Geological Society of America, Bulletin, v. 103, p. 1458–1475.

621 DeCelles, P.G., 2004, Late Jurassic to Eocene evolution of the Cordilleran thrust belt and foreland basin  
622 system, western U.S.A.: American Journal of Science, v. 304, p. 105–168.

623 Dickinson, W.R., Klute, M.A., Hayes, M.J., Janecke, S.U., Erik, R., Mckittrick, M.A., Olivares, M.D., Klute,  
624 M.A., and Hayes, M.J., 1988, Paleogeographic and paleotectonic setting of Laramide sedimentary  
625 basins in the central Rocky Mountain region: Geological Society of America, Bulletin, v. 100, p.  
626 1023–1039.

627 Dzombak, R., Midttun, N.C., Stein., R.A. and Sheldon, N.D., 2021, Incorporating lateral variability and  
628 extent of paleosols into proxy uncertainty: Palaeogeography, Palaeoclimatology,  
629 Paleoecology, v. 585, p. 1-12.

630 Duller, R.A., Armitage, J.J., Manners, H.R., Grimes, S., and Jones, T.D., 2019, Delayed sedimentary  
631 response to abrupt climate change at the Paleocene-Eocene boundary, northern Spain:  
632 *Geology*, v. 47, p. 159–162.

633 Fan, M., and Carrapa, B., 2014, Late Cretaceous – early Eocene Laramide uplift, exhumation, and  
634 basin subsidence in Wyoming: Crustal responses to flat slab subduction: *Tectonics*, v. 33, p.  
635 509–529.

636 Fielding, C.R., Allen, J.P., Alexander, J., and Gibling, M.G., 2009, Facies model for fluvial systems in the  
637 seasonal tropics and subtropics: *Geology*, v. 37, p. 623–626.

638 Foreman, B.Z., 2014, Climate-driven generation of a fluvial sheet sand body at the Paleocene-Eocene  
639 boundary in north-west Wyoming (USA): *Basin Research*, v. 26, p. 225–241.

640 Fricke, H.C., Clyde, W.C., O’Neil, J.R., and Gingerich, P.D., 1998, Evidence for rapid climate change in  
641 North America during the latest Paleocene thermal maximum: oxygen isotope compositions  
642 of biogenic phosphate from the Bighorn Basin (Wyoming): *Earth and Planetary Science  
643 Letters*, v. 160, p. 193–208.

644 Ganti, V. Hajek, E.A., Leary, K., Straub., K.M., and Paola, C., 2020, Morphodynamic hierarchy and the  
645 fabric of the sedimentary record: *Geophysical Research Letters*, v. 47, p. 1-10.

646 Gibling, M.R., 2006, Width and thickness of fluvial channel Bodies and valley fills in the geological  
647 record: A literature compilation and classification: *Journal of Sedimentary Research*, 76, p.  
648 731–770.

649 Gingerich, P.D., 2001, Biostratigraphy of the continental Paleocene-Eocene boundary interval on  
650 Polecat Bench in the northern Bighorn Basin, *In* Gingerich, P.D (ed) *Paleocene-Eocene*

651 Stratigraphy and Biotic change in the Bighorn Basin and Clarks Fork Basins, Wyoming:  
652 University of Michigan, Papers on Paleontology, v. 33, p. 37-71.

653 Gingerich, P.D., 2003, Mammalian responses to climate change at the Paleocene-Eocene boundary:  
654 Polecat Bench record in the northern Bighorn Basin, Wyoming, *in* Wing, S.L., Gingerich, P.D.,  
655 Schmitz, B., and Thomas, E., (eds.): Causes and Consequences of Globally Warm Climates in  
656 the Early Paleogene: Boulder, Colorado, Geological Society of America Special Paper 369, p.  
657 463–478. Gingerich, P.D., and Clyde, W.C., 2001, Overview of mammalian biostratigraphy in  
658 the Paleocene-Eocene Fort Union and Willwood Formations of the Bighorn and Clarks Fork  
659 Basins: University of Michigan Papers on Paleontology, v. 33, p. 1–14.

660 IPCC, 2021: Climate Change 2021: The Physical Science Basis. Contribution of Working Group I to the  
661 Sixth Assessment Report of the Intergovernmental Panel on Climate Change [Masson-  
662 Delmotte, V., P. Zhai, A. Pirani, S.L. Connors, C. Péan, S. Berger, N. Caud, Y. Chen, L. Goldfarb,  
663 M.I. Gomis, M. Huang, K. Leitzell, E. Lonnoy, J.B.R. Matthews, T.K. Maycock, T. Waterfield, O.  
664 Yelekçi, R. Yu, and B. Zhou (eds.)]. Cambridge University Press, Cambridge, United Kingdom  
665 and New York, NY, USA, 2391 .p.

666 IPCC, 2022: Climate Change 2022: Impacts, Adaptation and Vulnerability. Contribution of Working  
667 Group II to the Sixth Assessment Report of the Intergovernmental Panel on Climate Change  
668 [H.-O. Pörtner, D.C. Roberts, M. Tignor, E.S. Poloczanska, K. Mintenbeck, A. Alegría, M. Craig,  
669 S. Langsdorf, S. Löschke, V. Möller, A. Okem, B. Rama (eds.)]. Cambridge University Press.  
670 Cambridge University Press, Cambridge, UK and New York, NY, USA, 3056 .p.

671 Jerolmack, D.J., and Paola, C., 2010, Shredding of environmental signals by sediment transport:  
672 Geophysical Research Letters, v. 37, p. 1–5.

673 Jones, H.L.L., and Hajek, E.A., 2007, Characterizing avulsion stratigraphy in ancient alluvial deposits:  
674 Sedimentary Geology, v. 202, p. 124–137.

675 Knighton, D., 1998, Fluvial Forms and Processes: New Perspectives: Routledge, 400 p.

676 Kraus, M.J., 2001, Sedimentology and depositional setting of the Willwood Formation in the Bighorn  
677 and Clarks Fork Basins, *in* Gingerich, P.D. (ed): Paleocene-Eocene Stratigraphy and biotic  
678 Change in the Bighorn and Clarks Fork Basins, Wyoming, University of Michigan, Papers on  
679 Paleontology, V. 33, p. 15-28.

680 Kraus, M.J., McInerney, F.A., Wing, S.L., Secord, R., Baczynski, A.A., and Bloch, J.I., 2013,  
681 Paleohydrologic response to continental warming during the Paleocene–Eocene Thermal  
682 Maximum, Bighorn Basin, Wyoming: Palaeogeography, Palaeoclimatology, Palaeoecology, v.  
683 370, p. 196–208.

684 Kraus, M.J., and Wells, T.M., 1999, Recognizing avulsion deposits in the ancient stratigraphical record,  
685 *in* Smith, N.D. and Rogers, J. (eds), Fluvial Sedimentology 6: Special Publication of the  
686 International Association of Sedimentologists, p. 251–268.

687 Kraus, M.J., and Riggins, S., 2007, Transient drying during the Paleocene–Eocene Thermal Maximum  
688 (PETM): Analysis of paleosols in the bighorn basin, Wyoming: Palaeogeography,  
689 Palaeoclimatology, Palaeoecology, v. 245, p. 444–461.

690 Kraus, M.J., Woody, D.T., Smith, J.J., and Dukic, V., 2015, Alluvial response to the Paleocene–Eocene  
691 Thermal Maximum climatic event, Polecat Bench, Wyoming (U.S.A.): Palaeogeography,  
692 Palaeoclimatology, Palaeoecology, v. 435, p. 177–192, doi:10.1016/j.palaeo.2015.06.021.



693 Leopold, L.B., and Maddock, T., 1953, The Hydraulic Geometry of Stream Channels and Some  
694 Physiographic Implications: US Geological Survey, Professional Paper 252, 64 p.

695 Mackin, J.H., 1948, Concept of the graded river: Geological Society of America Bulletin, V. 59, p. 463-  
696 512.

697 Macklin, M.G., Fuller, I.C., Lewin, J., Maas, G.S., Passmore, D.G., Rose, J., Woodward, J.C., Black, S.,  
698 Hamlin, R.H.B., and Rowan, J.S., 2002, Correlation of fluvial sequences in the Mediterranean  
699 basin over the last 200 ka and their relationship to climate change: Quaternary Science  
700 Reviews, v. 21, p. 1633–1641.

701 Macklin, M.G., Lewin, J., and Woodward, J.C., 2012, The fluvial record of climate change: Royal  
702 Society of London Philosophical Transactions A: Mathematical, Physical and Engineering  
703 Sciences, v. 370, p. 2143–2172.

704 McNerney, F.A., and Wing, S.L., 2011, The Paleocene-Eocene Thermal Maximum: A Perturbation of  
705 Carbon Cycle, Climate, and Biosphere with Implications for the Future: Annual Review of  
706 Earth and Planetary Sciences, v. 39, p. 489–516.

707 Nanson, G.C., Cohen, T.J., Doyle, C.J. and Price, D.M., 2003, Alluvial evidence of major late Quaternary  
708 climate and flow-regime changes on the coastal rivers of New South Wales, Australia, *in*: Gregory,  
709 K. and Benito, G (eds.): Palaeohydrology: Understanding Global Change: John Wiley and  
710 Sons, Chichester, p. 233– 258.

711 Middleton, G.V., 1973, Johannes Walther’s Law of the Correlation of Facies: Geological Society of  
712 America, Bulletin, V. 84, p. 979-988.

713 Owen, A., Ebinghaus, A., Hartley, A.J., Santos, M.G.M., and Weissmann, G.S., 2017, Multi-scale  
714 classification of fluvial architecture: An example from the Palaeocene-Eocene Bighorn Basin,  
715 Wyoming: *Sedimentology*, v. 64, p. 1572-1596.

716 Owen, A., Hartley, A.J., Ebinghaus, A., Weissmann, G.S., and Santos, M.G.M., 2019, Basin-scale  
717 predictive models of alluvial architecture: Constraints from the Palaeocene–Eocene, Bighorn  
718 Basin, Wyoming, USA: *Sedimentology*, v. 66, p. 736–763.

719 Pancost, R.D., 2017, Climate change Narratives: *Nature Geoscience*, v. 10, p. 466-468.

720 Paola, C., Ganti, V., Mohrig, D., Runkel., A.C., and Straub, K.M., 2018, Time not our time: Physical  
721 controls on the preservation and measurement of geologic time: *Annual Review of Earth and*  
722 *Planetary Sciences*, V. 46, p. 409-438.

723 Plink-Björklund, P., 2015, Morphodynamics of rivers strongly affected by monsoon precipitation:  
724 Review of depositional style and forcing factors: *Sedimentary Geology*, v. 323, p. 110-147.

725 Rose, K.D., Chew, A.E., Dunn, R.H., Kraus, M.J., Fricke, H.C., and Zack, S.P. 2012, Earliest Eocene  
726 Mammalian Fauna from the Paleocene-Eocene Thermal Maximum at Sand Creek Divide,  
727 Southern Bighorn Basin, Wyoming: *University of Michigan, Papers on Paleontology* v. 36). P.  
728 1-14.

729 Rouse, J.T., 1937, Genesis and structural relationships of the Absaroka volcanic rocks, Wyoming:  
730 *Geological Society of America Bulletin* , v. 48, p. 1257–1296.

731 Ruhe, R.V. and Olson, C.G. 1980 Soil Welding: *Soil Science*, v. 130, p. 132-139.

732 Sadler, P.M., 1981, Sediment Accumulation Rates and the Completeness of Stratigraphic Sections:  
733 *Journal of Geology*, v. 89, p. 569–584.

734 Schmitz, B., and Pujalte., V., 2003, Sea-level, humidity, and land-erosion records across the initial  
735 Eocene thermal maximum from a continental-marine transect in northern Spain: *Geology*, v  
736 31, p.689-692.

737 Schumm, S.A., 1979, *Geomorphic Thresholds: The Concept and Its Applications*: Institute of British  
738 Geographers Transactions, v. 4, p. 485-515.

739 Seeland, D., 1998, Late Cretaceous , Paleocene, and Early Eocene Paleogeography of the Bighorn  
740 Basin and Northwestern Wyoming, *in*: *Cretaceous and Lower tertiary Rocks of the Bighorn*  
741 *Basin, Wyoming and Montana; 49th Annual Field Conference Guidebook*, 1–29.

742 Simpson, G., and Castellort, S., 2012, Model shows that rivers transmit high-frequency climate cycles  
743 to the sedimentary record: *Geology*, v. 40, p. 1131–1134.

744 Slater, L.J., and Singer, M.B., 2013, Imprint of climate and climate change in alluvial riverbeds:  
745 *Continental United States, 1950-2011*: *Geology*, v. 41, p. 595–598.

746 Smith, J.J., Hasiotis, S.T., Kraus, M.J., and Woody, D.T., 2008, Relationship of Floodplain  
747 Ichnocoenoses to Paleopedology, Paleohydrology, and Paleoclimate in the Willwood  
748 Formation, Wyoming, During the Paleocene-eocene Thermal Maximum: *Palaios*, v. 23, p.  
749 683–699.

750 Snell, K.E., Thrasher, B.L., Eiler, J.M., Koch, P.L., Sloan, L.C., and Tabor, N.J., 2013, Hot summers in the  
751 Bighorn Basin during the early Paleogene: *Geology*, v. 41, p. 55–58.

752 Snyder, W.S., Dickinson, W.R. and Silberman, M.L., 1976, Tectonic implications of space-time patterns  
753 of Cenozoic magmatism in the Western United States: *Earth and Planetary Science Letters*, v.  
754 32, p. 91-106.

755 Starkel, L., 1991, Environmental changes at the Younger Dryas-Preboreal transition and during the  
756 early Holocene: Some distinctive aspects in central Europe: *The Holocene*, v. 1, p. 234–242.

757 Straub, K.M., Duller, R.A., Foreman, B.Z., and Hajek, E.A., 2020, Buffered, Incomplete, and Shredded:  
758 The Challenges of Reading an Imperfect Stratigraphic Record: *Journal of Geophysical*  
759 *Research: Earth Surface*, v. 125, p. 1–44.

760 Sundell, K.A., 1990, Sedimentation and tectonics of the Absaroka Basin of northwestern Wyoming, *in*  
761 *Wyoming sedimentation and Tectonics, 41st Annual Field Conference Guidebook*, p. 105–122.

762 Toby, S.C., Duller, R.A., Angelis, S.D., and Straub, K.M., 2022, Morphodynamics limits to  
763 environmental signal propagation across landscape and into strata: *Nature Communications*,  
764 v. 12., 10. p.

765 Vandenberghe, J., 2002, the relation between climate and river processes, landforms and deposits  
766 during the Quaternary: *Quaternary International*, V.91, p.17-23.

767 Van Houten, F.B., 1944, Stratigraphy of the Willwood and Tatman Formations in northwestern  
768 Wyoming: *Geological Society of America 1987 Annual Meeting and Exposition Program*, v. 55,  
769 p. 165–210.

770 Welch, J.L., Foreman, B.Z., Malone, D., and Craddock, J., 2022, Provenance of early Paleogene strata  
771 in the Bighorn Basin (Wyoming, USA): Implications for Laramide tectonism and basin-scale  
772 stratigraphic patterns, *in* Craddock, J.P., Malone, D.H., Foreman, B.Z., and Konstantinou, A.,  
773 (eds), *Tectonic Evolution of the Sevier-Laramide Hinterland, Thrust Belt, and Foreland, and*  
774 *Postorogenic Slab Rollback (180–20 Ma): Geological Society of America, Special Paper 555*, p.  
775 241–264

776 Whipple, K.X., 2001, Fluvial landscape response time: how plausible is steady-state denudation:  
777 American Journal of Science, v. 301, p. 313–325.

778 Willis, B.J., and Behrensmeyer, A.K., 1995, Fluvial systems in the Siwalik Miocene and Wyoming  
779 Paleogene: Palaeogeography, Palaeoclimatology and Palaeoecology, v. 115, p. 13-35.

780 Wing, S.L., and Currano, E.D., 2013, Plant response to a global greenhouse event 56 million years ago:  
781 American Journal of Botany, v. 100, p. 1234–54.

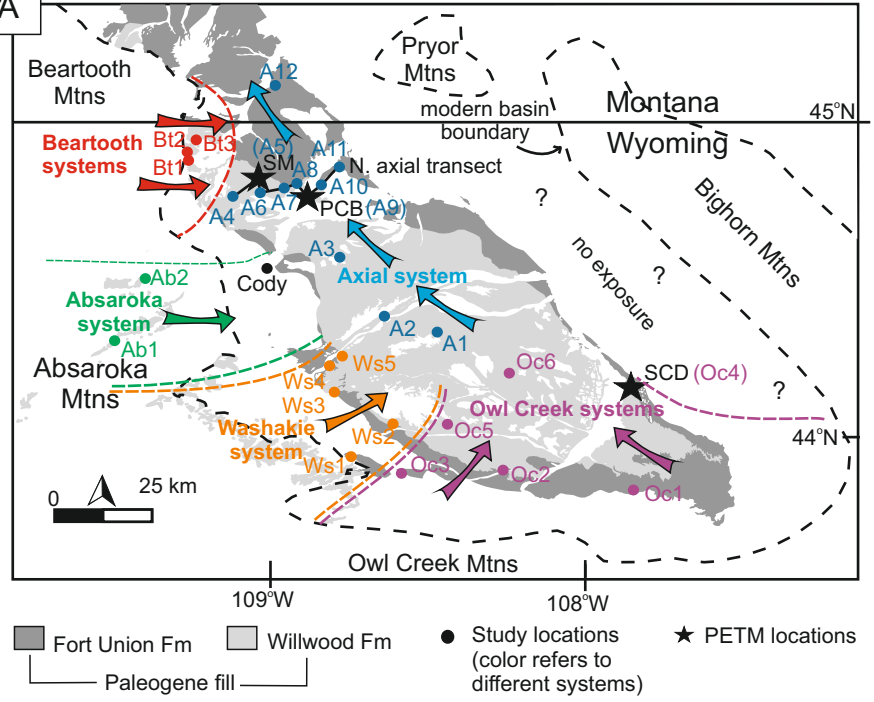
782 Wing, S.L., Harrington, G.J., Smith, F.A., Bloch, J.I., Boyer, D.M., and Freeman, K.H., 2005, Transient  
783 floral change and rapid global warming at the Paleocene-Eocene boundary: Science, v. 310, p.  
784 993–6.

785 Yuretich, R.F., Hickey, L.J., Gregson, B.P., and Hsia, Y.L., 1984, Lacustrine deposits in the Paleocene  
786 Fort Union Formation, northern Bighorn Basin, Montana: Journal of Sedimentary Petrology, v.  
787 54, p. 836–852.

788 Zachos, J.C., Wara, M.W., Bohaty, S., Delaney, M.L., Petrizzo, M.R., Brill, A., Bralower, T.J., and  
789 Premoli-Silva, I., 2003, A transient rise in tropical sea surface temperature during the  
790 Paleocene-Eocene Thermal Maximum: Science, v. 302, p. 1551-1554.

791 Zachos, J.C., Röhl, U., Schellenberg, S.A., Sluijs, A., Hodell, D.A., Kelly, D.C., Thomas, E., Nicolo, M.,  
792 Raffi, I., Lourens, L.J., McCarren, H., Kroon, D. 2005, Rapid acidification of the ocean during the  
793 Paleocene-Eocene Thermal Maximum: Science, v. 308, p. 1611–1616.

Figure 1



B

Epoch	Age (N.America)	Formation
Eocene		No strat
		Bridgerton
		Tatman Fm
	Wasatchian	Willwood Fm
Paleocene	Clarkforkian	
	Tiffanian	Fort Union Fm
	Torrajonian	
	Puercan	



Figure 3

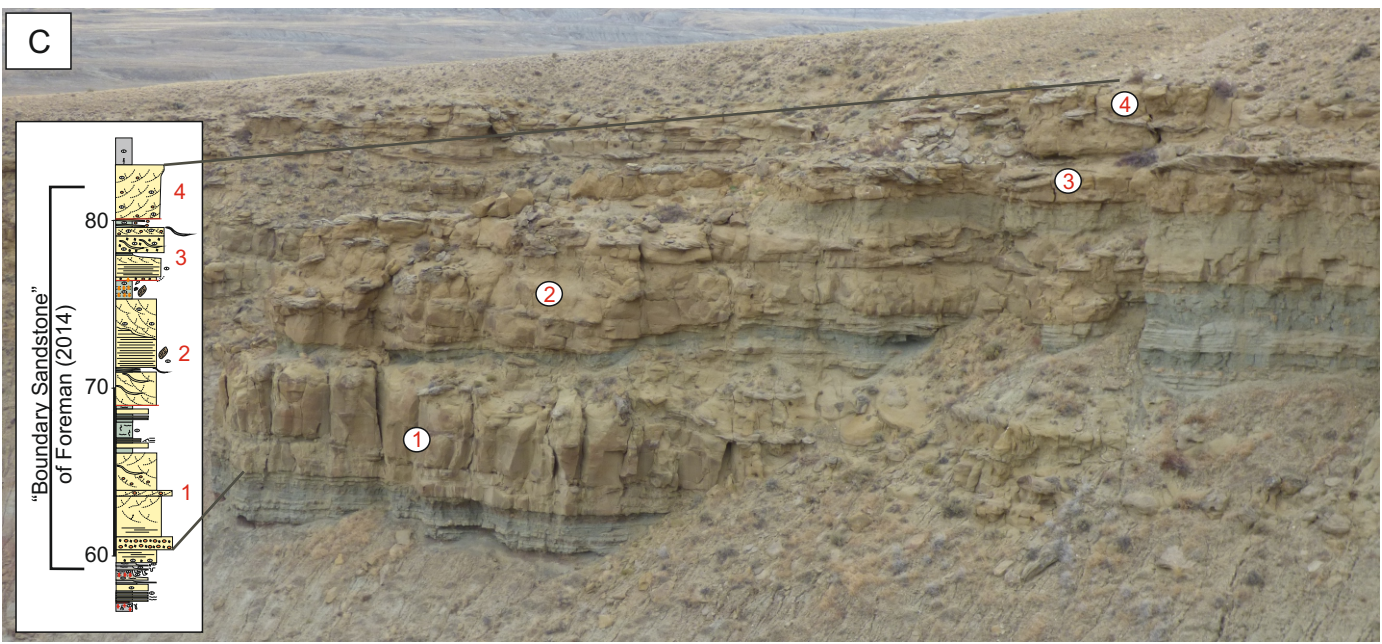
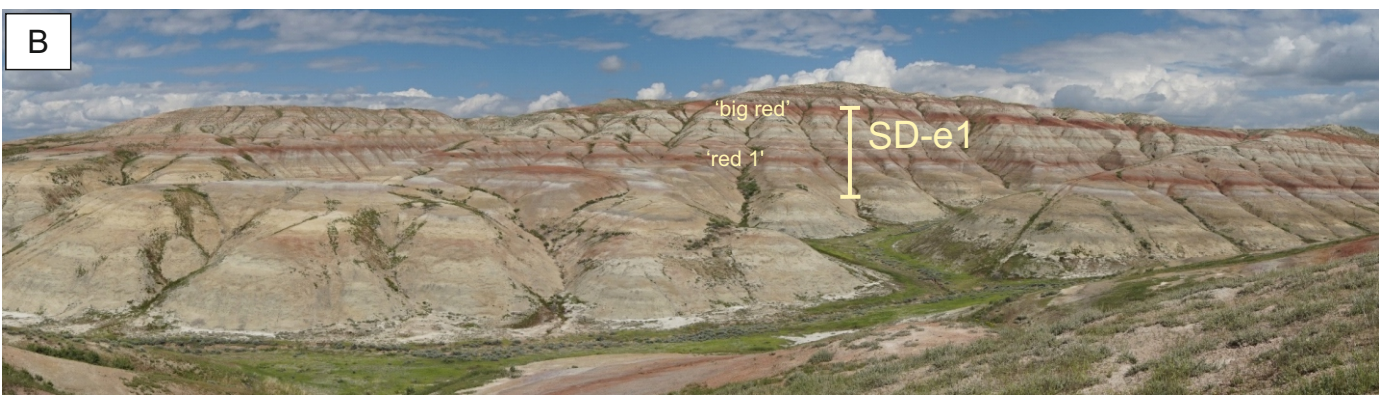
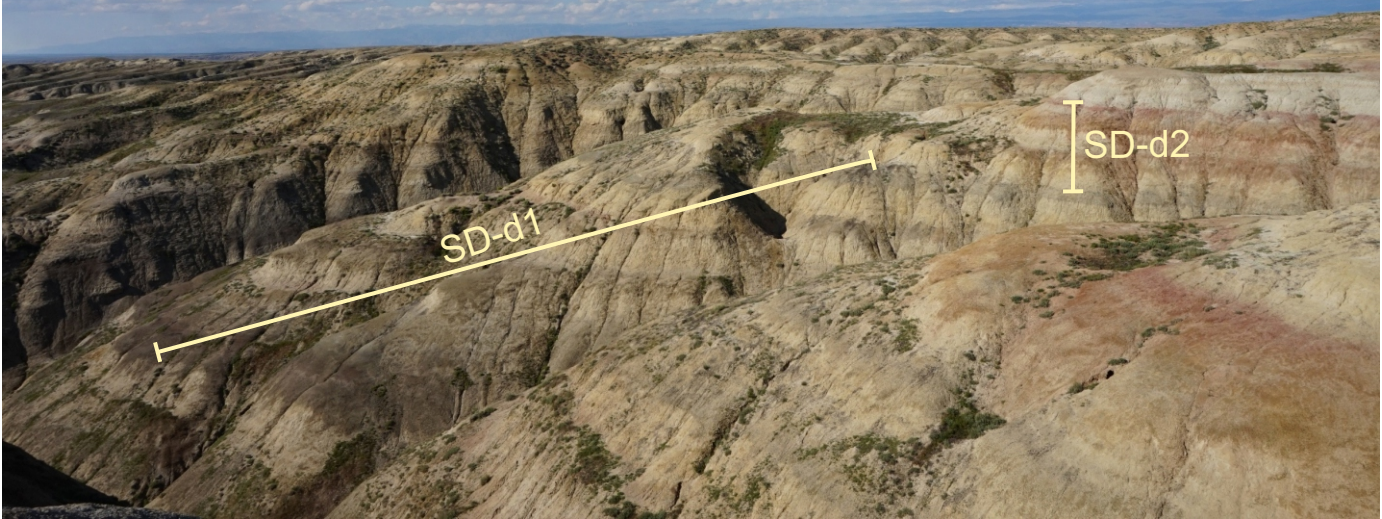
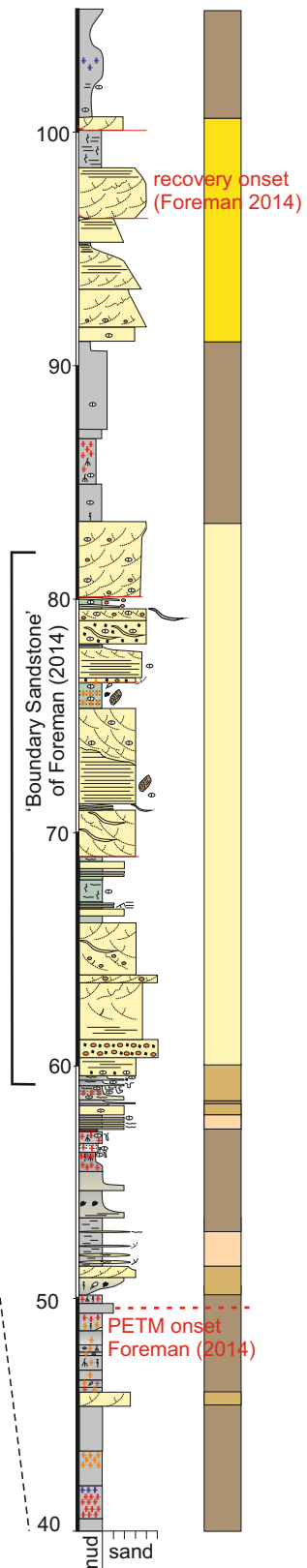
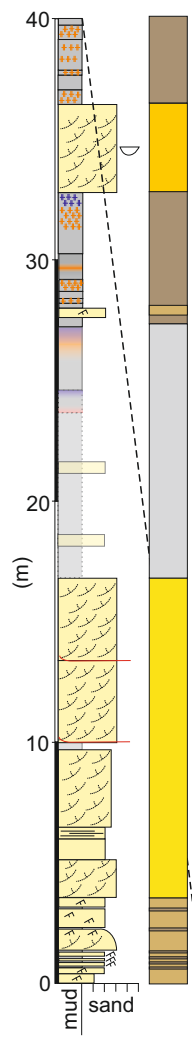
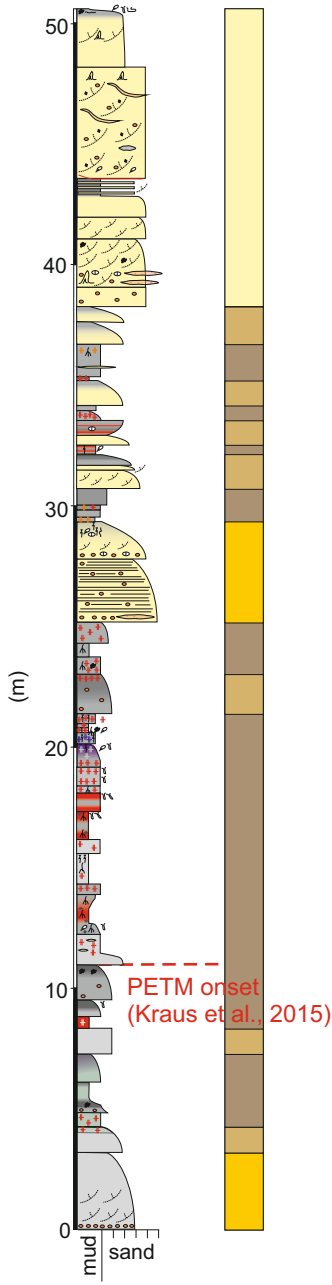




Figure 4 Polecat Bench

B



**Key**

- |                                       |                             |
|---------------------------------------|-----------------------------|
| trough cross-bedding                  | wood fragments              |
| current ripples                       | rooting                     |
| soft sediment deformation             | burrows                     |
| wavy lamination                       | CaCO <sub>3</sub> nodules   |
| horizontal lamination/bedding         | slickensides                |
| accretion surfaces                    | plant fragments             |
| ribbon geometry                       | organic matter              |
| gravel pockets                        | mottling                    |
| gravel sized clasts                   | mud clasts                  |
| Internally Amalgamated channel facies |                             |
| Offset stacked channel facies         | Floodplain - sand dominated |
| Isolated channel facies               | Floodplain - heterolithic   |
| Floodplain - mud dominated            | Floodplain - inferred       |

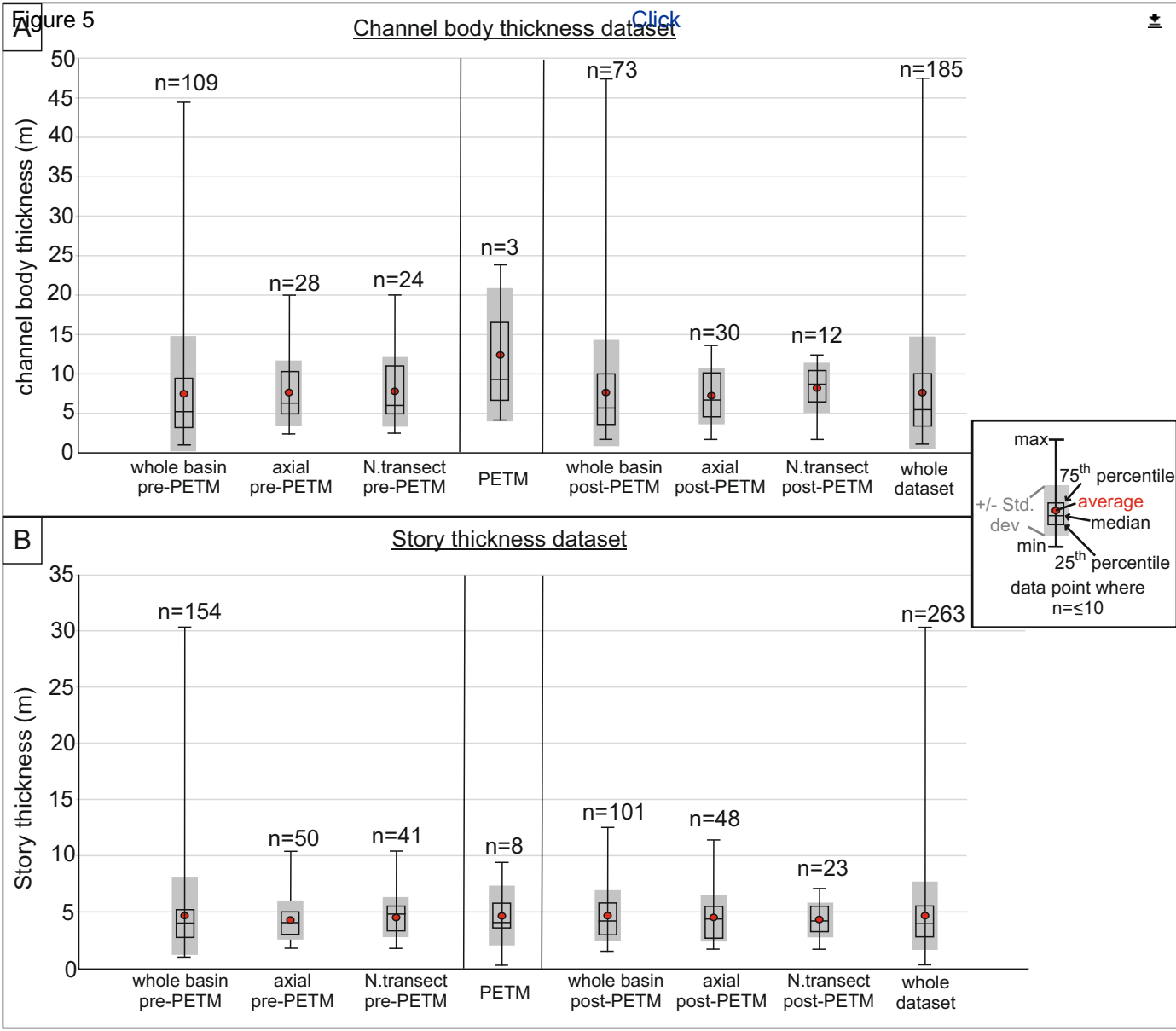


Figure 6

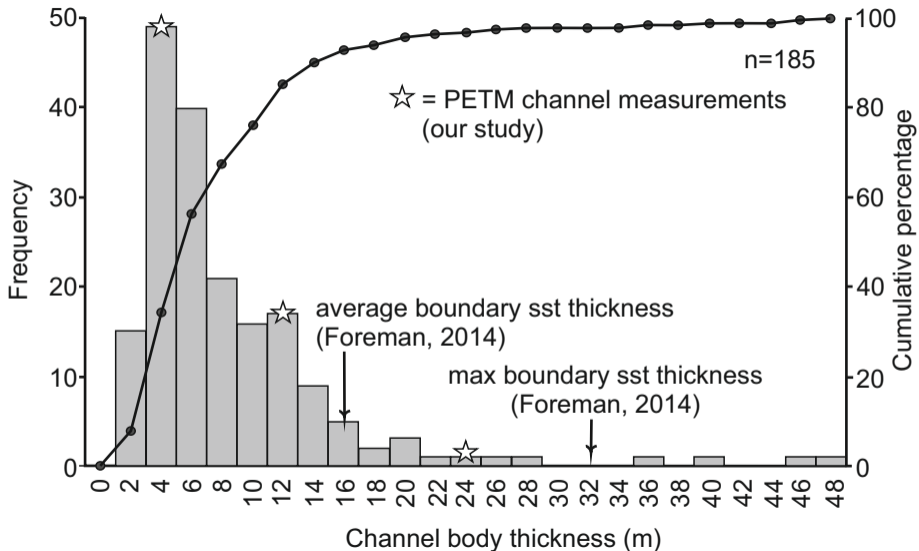
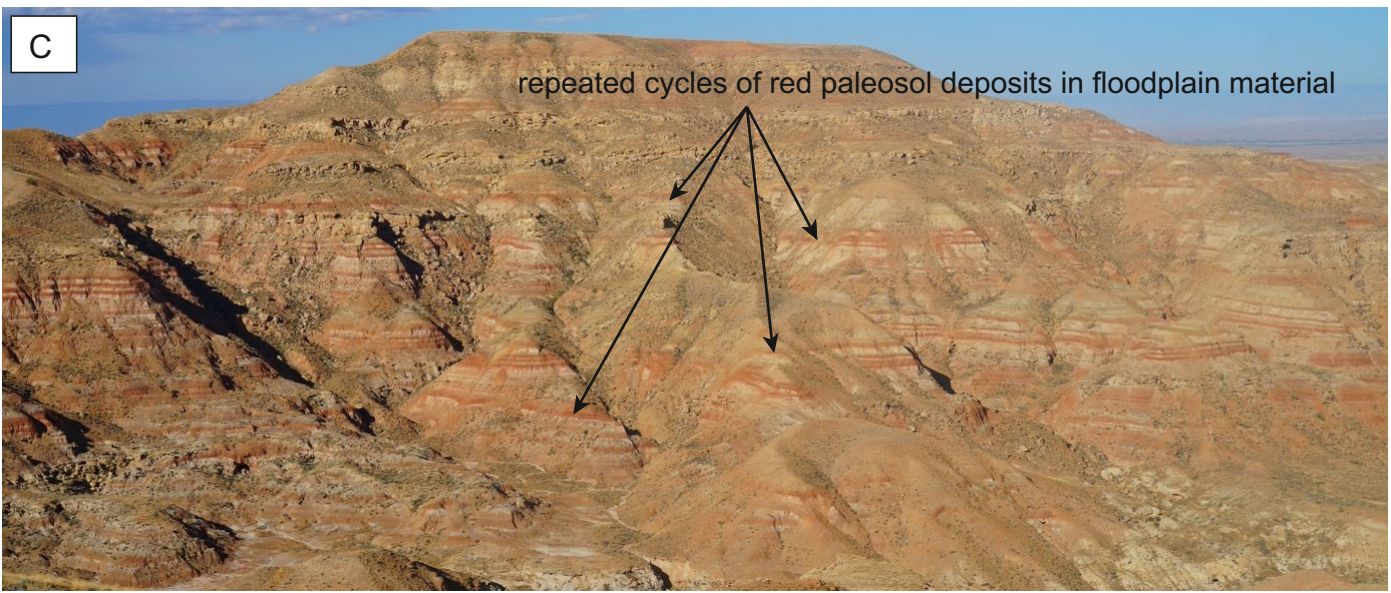
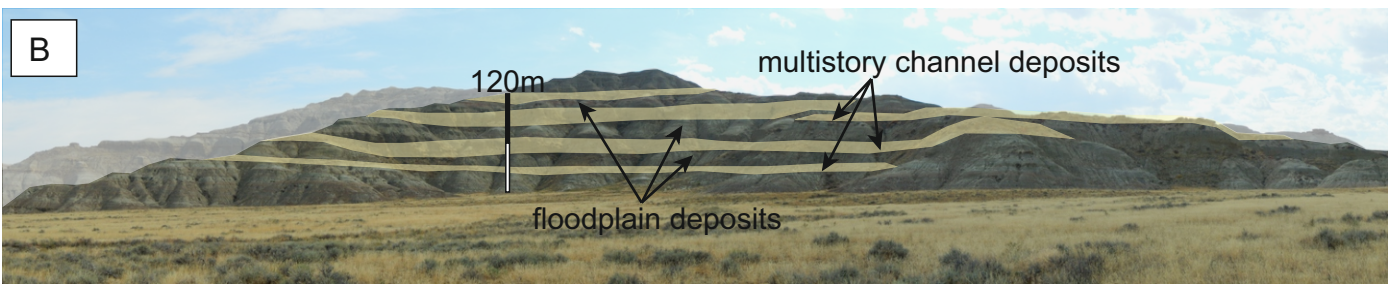
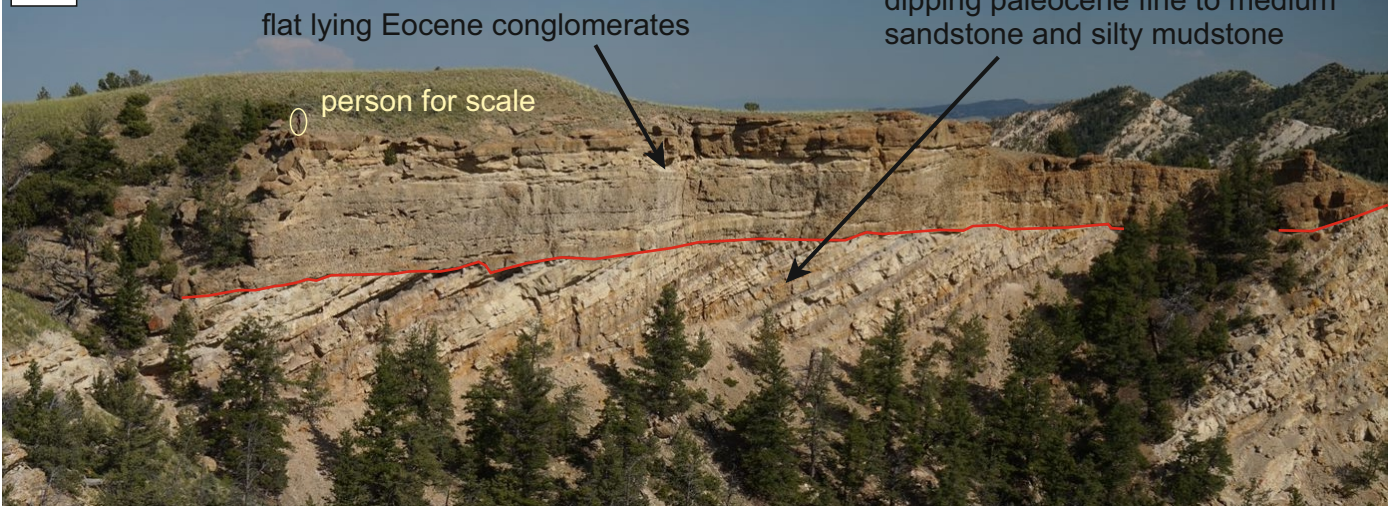


Figure 7



**Table 1.** Summary of key characteristics and examples of pre-PETM, PETM, and post-PETM within the Bighorn Basin. Please see references for full details, examples and broad trends given in Table 1.

	Pre-PETM	PETM	Post-PETM
<b>Mean annual temperature (MAT; °C)</b> (LMA, Wing et al., 2005)	15.7 ± 2.4 (Wing et al. 2005)	Increase of approximately 5 19.8 ± 3.1 (Wing et al. 2005)	18.2 ± 2.3 (Wing et al. 2005)
<b>Mean annual precipitation (MAP; mm)</b> (LMA - Wing et al., 2005); CIA-K Paleosol analysis. Kraus and Riggins, 2007; Kraus et al., 2015)	1139-1163 ± 108 (Kraus and Riggins, 2007) 1153-1208 ± 108 (Kraus et al. 2015)	800+1140/-560 & 410 for base PETM. 1440 + 2060/-1000 & 1320 upper PETM (Wing et al., 2005) 755-1186 ± 108 (Kraus and Riggins, 2007) 516-1157 ± 108 (Kraus et al. 2015)	Pre-PETM values (e.g. 820-1036 ± 108; Kraus et al. 2015).
<b>Vegetation type</b> (Wing et al., 2005; Smith et al., 2008; McInerney and Wing, 2011; Kraus et al., 2013)	Deciduous and evergreen broad-leaved taxa, conifers in the bald cypress family. Mesic temperate environments	Lacks conifers, dominated by bean family. Dry tropical and subtropical setting.	Pre-PETM conditions
<b>Vegetation density</b> (Wing et al., 2005; Smith et al., 2008)	Dense forest structure	Relatively open/less dense forest structure	Pre-PETM conditions
<b>Mammalian fauna</b> (Gingerich, 2003)	<i>Champsosaurus</i> , Plesiadapidae. Appearance of Rodentia, Tillodontia, <i>Haplomyli</i> in the <i>Clarksforkian</i> .	"Dwarfing" of mammals. Appearance of new species e.g., the condylarth, the pantodont <i>Coryphodon</i> . Disappearance of <i>Champsosaurus</i> , Plesiadapidae.	Some species recover, some permanently change ("evolutionary change"). First appearance of cosmopolitan Perissodactyla, Artiodactyla, Primates, and hyaenodontid
<b>Paleosols</b> (Kraus and Riggins, 2007; Kraus et al., 2013; 2015)	Dominantly gray, intermittent thin purple/red paleosols.	More welded and thicker red, yellow-brown	Intermediate paleosols. More widely spaced paleosols

**Table 2** Summary descriptions of facies associations observed in the Paleocene and Eocene fill of the Bighorn Basin (see Owen et al., 2017 for full descriptions of facies and geometries.).

<b>Channel body geometries (Owen et al., 2017)</b>	<b>Massive</b>	Large, broad channel geometry. Rare story surfaces that are spatially isolated
	<b>Semi Amalgamated</b>	Semi-amalgamated with other channel deposits. Channel body can have irregular geometries. Story surfaces are present to varying degrees, can be crosscutting one another or spatially isolated.
	<b>Internally amalgamated</b>	Broad tabular geometry that laterally pinches out. Story surfaces are prevalent, can be crosscutting one another, or spatially isolated.
	<b>Offset stacked</b>	A broad tabular geometry. However, stories are offset from one another, leaving an irregular edge to the channel body. Single story across most of the channel body, multistory across minor portions at amalgamation points.
	<b>Isolated</b>	Channel geometry that pinches out laterally. Can be asymmetrical or symmetrical. Single story.
<b>Channel facies association (Owen et al., 2017)</b>	<b>Gravelly braided stream</b>	Conglomerates composed of granule- to boulder-sized, well-rounded, moderately sorted. Imbrication, fining-up sequences, sandstone lenses, accretion surfaces and parallel stratification can be present. Matrix composed of silt to coarse sand. Channel body can be either massive or semi-amalgamated.
	<b>Heterolithic, dominantly braided</b>	Medium- to cobble-dominated sandstone that are moderate to poorly sorted. Parallel lamination, trough cross bedding and accretion surfaces (dominantly downstream) present. Channel body can be Internally amalgamated, semi-amalgamated, or have massive geometries
	<b>Heterolithic, dominantly meandering</b>	Dominantly medium to fine sandstone. Well-sorted with area with material (mud, granules, or nodules) lining trough cross sets. Upper and lower plane-bed lamination, current ripples, accretion packages (dominantly lateral) and soft-sediment deformation present. Mudstone present in some heterolithic accretion packages. Channel bodies can have a semi-amalgamated, internally amalgamated, or offset-stacked geometry.
	<b>Fine-grained channel fill</b>	Silt to medium sandstone with deposits being either heterolithic, or sand- or mud-dominated. Current ripples, trough cross bedding and parallel lamination present. Rare accretion surfaces (dominantly lateral). Channel bodies can have an internally amalgamated, offset stacked or isolated geometry.
<b>Floodplain deposits (Owen et al., 2017)</b>	<b>Minor lacustrine</b>	Mud- to sand-dominated sequences with horizontal lamination, current ripples, bioturbation, and trough cross stratification present to varying degrees. Rare limestone beds with wavy lamination.
	<b>Paleosols</b>	Two broad paleosols types observed. Well-drained paleosols are dominantly red and composed of clay to fine to medium sandstone. Rootlets, rhizoliths, carbonate nodules, slickensides, mottling, organic matter and bioturbation all observed. Poorly drained deposits are gray, green, and purple and composed of clay to fine-medium sandstone. Structures include rootlets, slickensides, mottling, and burrows, but to a lesser degree than the well-drained paleosols, with the exception of organic matter, which is more prevalent in the poorly drained facies.
	<b>Splay and sheet floods</b>	Composed of minor channel (ribbon) and sheet deposits composed of fine to coarse sands that are well sorted. Structures present include parallel and ripple lamination and minor trough cross bedding as well as evidence of bioturbation.



**Table 3** Summary data (in meters) for channel body and storey deposits pre-PETM, PETM and post-PETM for the whole basin, whole axial system and northern basin transect. See Figure 5 for graphical representation of dataset.

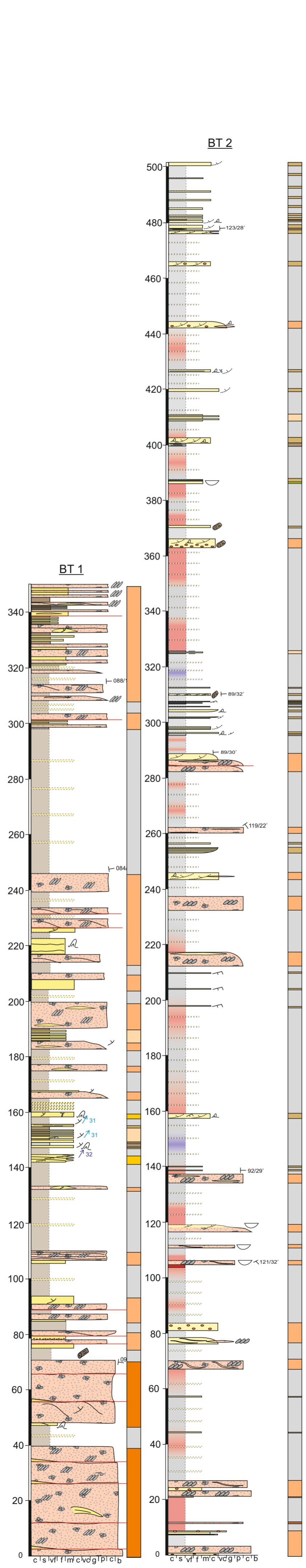
Channel bodies								
	whole Basin Pre-PETM	whole axial pre-PETM)	north basin pre-PETM	PETM	whole basin post-PETM	axial post-PETM	north basin post-PETM	Entire dataset
Average thickness (m)	7.49	7.65	7.75	12.40	7.66	7.19	8.25	7.64
Max thickness (m)	44.50	20.00	20.00	23.80	47.50	13.70	12.40	47.50
Min thickness (m)	1.00	2.40	2.40	4.10	1.70	1.70	1.70	1.00
Upper stdv (m)	14.71	11.71	12.08	20.74	14.27	10.64	11.34	14.67
Lower stdv (m)	0.27	3.59	3.42	4.06	1.04	3.74	5.16	0.60
Q1 (m)	3.20	4.95	4.95	6.70	3.60	4.53	6.48	3.40
Median (m)	5.20	6.30	6.00	9.30	5.70	6.75	8.70	5.50
Q3 (m)	9.40	10.25	11.00	16.55	10.10	10.15	10.40	10.00
Stories								
	whole Basin Pre-PETM	whole axial pre-PETM)	north basin pre-PETM	PETM	whole basin post-PETM	axial post-PETM	north basin post-PETM	Entire dataset
Average thickness (m)	4.67	4.29	4.54	4.65	4.67	4.50	4.30	4.67
Max thickness (m)	30.30	10.40	10.40	9.40	12.50	11.40	7.10	30.30
Min thickness (m)	1.00	1.80	1.80	0.30	1.50	1.70	1.70	0.30
Upper stdv (m)	8.08	5.96	6.26	7.24	6.87	6.46	5.77	7.64
Lower stdv (m)	1.26	2.61	2.81	2.06	2.47	2.53	2.84	1.69
Q1 (m)	2.73	3.00	3.30	3.60	3.00	2.75	3.25	3.00
Median (m)	4.00	4.05	4.80	4.05	4.20	4.40	4.20	4.00
Q3 (m)	5.20	5.00	5.50	5.75	5.80	5.50	5.50	5.50



**Table 4.** Summary statistical results comparing pre-PETM and PETM channel depths (storey thicknesses). Results are presented for two assumptions for standard deviations, s.d., for the PETM data: (1) s.d. calculated from all 8 available measurements; (2) s.d. estimated as being the same as in the larger pre-PETM data sets for the same locations. The channel-forming discharge estimates were calculated using  $f=0.4$  in an empirical relationship between channel depth,  $h$ , and discharge,  $Q$ ,  $h=cQ^f$ .

	Northern Axial		Axial	
	Pre-PETM	PETM	Pre-PETM	PETM
Number of measurements, N	41	8	50	8
Mean $\bar{x}$ [m]	4.54	4.65	4.29	4.65
Standard deviation $\sigma$ [m]	1.73	2.77	1.68	2.77
Standard error, s.e., $(\bar{x}/\sqrt{N})$ [m]	0.27	0.98	0.24	0.98
Pooled s.e. (measured / estimated PETM $\sigma$ )	1.01 / 0.67		1.01 / 0.64	
t-values (calculated / critical at 95% confidence)	0.11 / 1.90		0.36 / 1.90	
Minimum PETM storey thickness for 95% significant increase (using measured / estimated PETM $\sigma$ )	6.46 / 5.80		6.19 / 5.49	
Ratio of channel-forming discharge $Q$ during PETM to pre-PETM to produce 95% significant channel depth increase (using measured / estimated PETM $\sigma$ )	2.42 / 1.85		2.51 / 1.86	

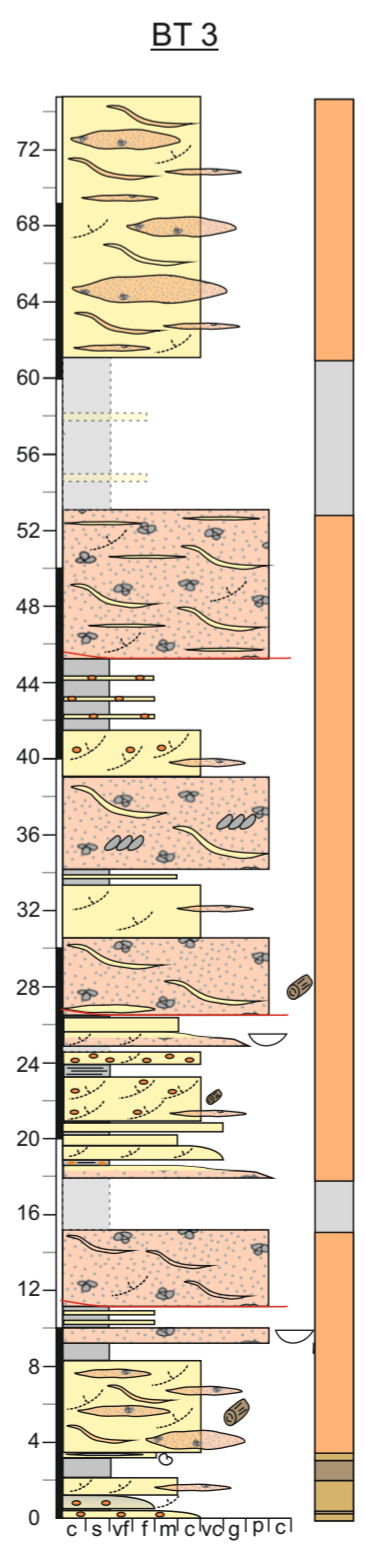
**Beartooth fluvial systems**



**KEY**

- |  |                           |  |                          |  |                                       |
|--|---------------------------|--|--------------------------|--|---------------------------------------|
|  | current ripples           |  | wood debris              |  | Massive channel facies                |
|  | horizontal lamination     |  | rootlets                 |  | Semi-Amalgamated channel facies       |
|  | trough cross-bedding      |  | vertical burrow          |  | Internally Amalgamated channel facies |
|  | wavy lamination           |  | sub-horizontal burrow    |  | Offset stacked channel facies         |
|  | slumping                  |  | horizontal burrow        |  | Isolated channel facies               |
|  | imbricated clasts         |  | groove                   |  | Floodplain - mud dominated            |
|  | accretion surface         |  | bone material            |  | Floodplain - sand dominated           |
|  | gravel lense              |  | shell material           |  | Floodplain - heterolithic             |
|  | sand lense                |  | slickensides             |  | Floodplain channel (splay)            |
|  | soft sediment deformation |  | calcium carbonate nodule |  | Floodplain- inferred                  |
|  | mud clast                 |  | leaf material            |  |                                       |
|  | outsized clast            |  | mottling                 |  |                                       |
|  | granule                   |  | organic material         |  |                                       |
|  | channel geometry          |  |                          |  |                                       |
|  | gradational boundary      |  |                          |  |                                       |
|  | storey surface            |  |                          |  |                                       |

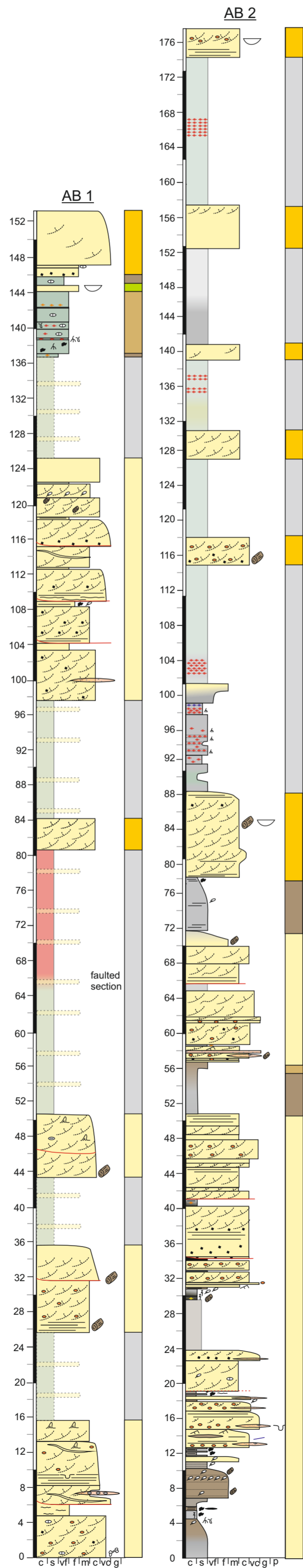
Please see Owen et al. 2017 for full facies descriptions



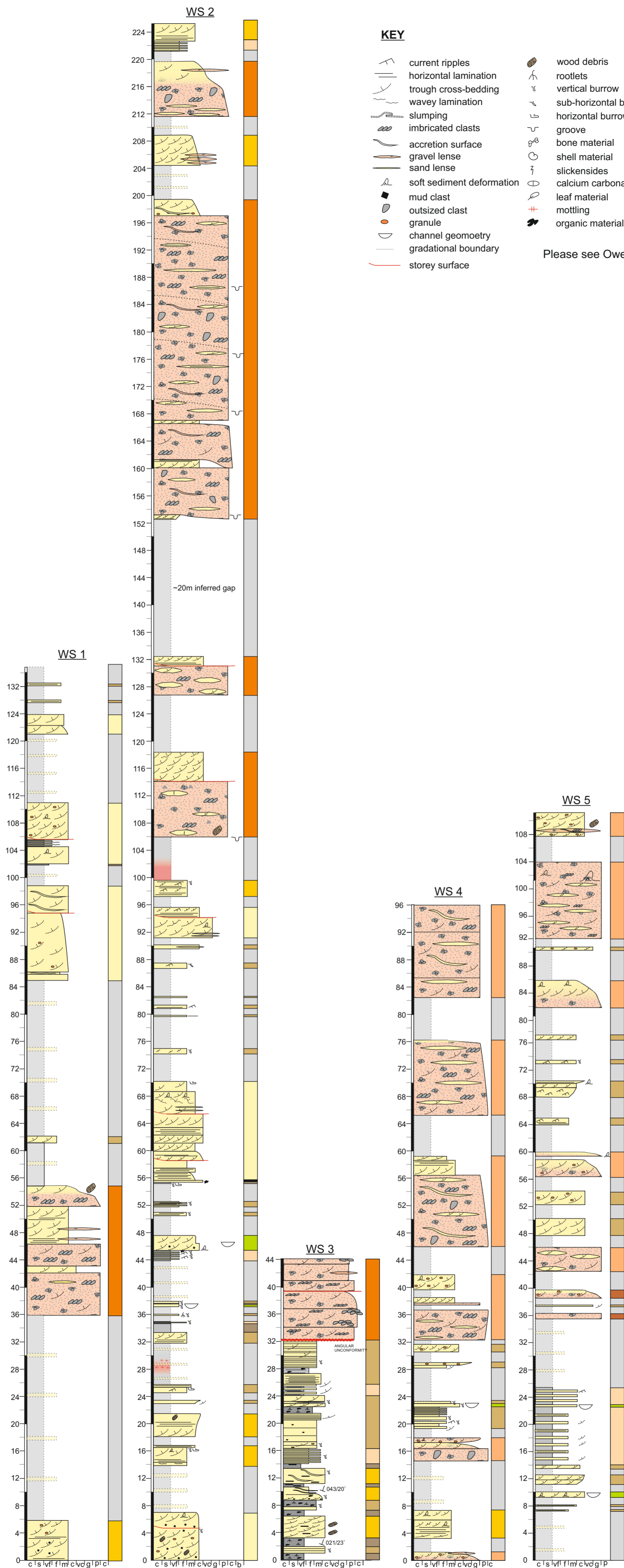
# Absoraka fluvial systems

## KEY

- |  |                           |  |                          |  |                                       |
|--|---------------------------|--|--------------------------|--|---------------------------------------|
|  | current ripples           |  | wood debris              |  | Massive channel facies                |
|  | horizontal lamination     |  | rootlets                 |  | Semi-Amalgamated channel facies       |
|  | trough cross-bedding      |  | vertical burrow          |  | Internally Amalgamated channel facies |
|  | wavy lamination           |  | sub-horizontal burrow    |  | Offset stacked channel facies         |
|  | slumping                  |  | horizontal burrow        |  | Isolated channel facies               |
|  | imbricated clasts         |  | groove                   |  | Floodplain - mud dominated            |
|  | accretion surface         |  | bone material            |  | Floodplain - sand dominated           |
|  | gravel lense              |  | shell material           |  | Floodplain - heterolithic             |
|  | sand lense                |  | slickensides             |  | Floodplain channel (splay)            |
|  | soft sediment deformation |  | calcium carbonate nodule |  | Floodplain- inferred                  |
|  | mud clast                 |  | leaf material            |  |                                       |
|  | outsized clast            |  | mottling                 |  |                                       |
|  | granule                   |  | organic material         |  |                                       |
|  | channel geometry          |  |                          |  |                                       |
|  | gradational boundary      |  |                          |  |                                       |
|  | storey surface            |  |                          |  |                                       |
- Please see Owen et al. 2017 for full facies descriptions



Washakie fluvial systems

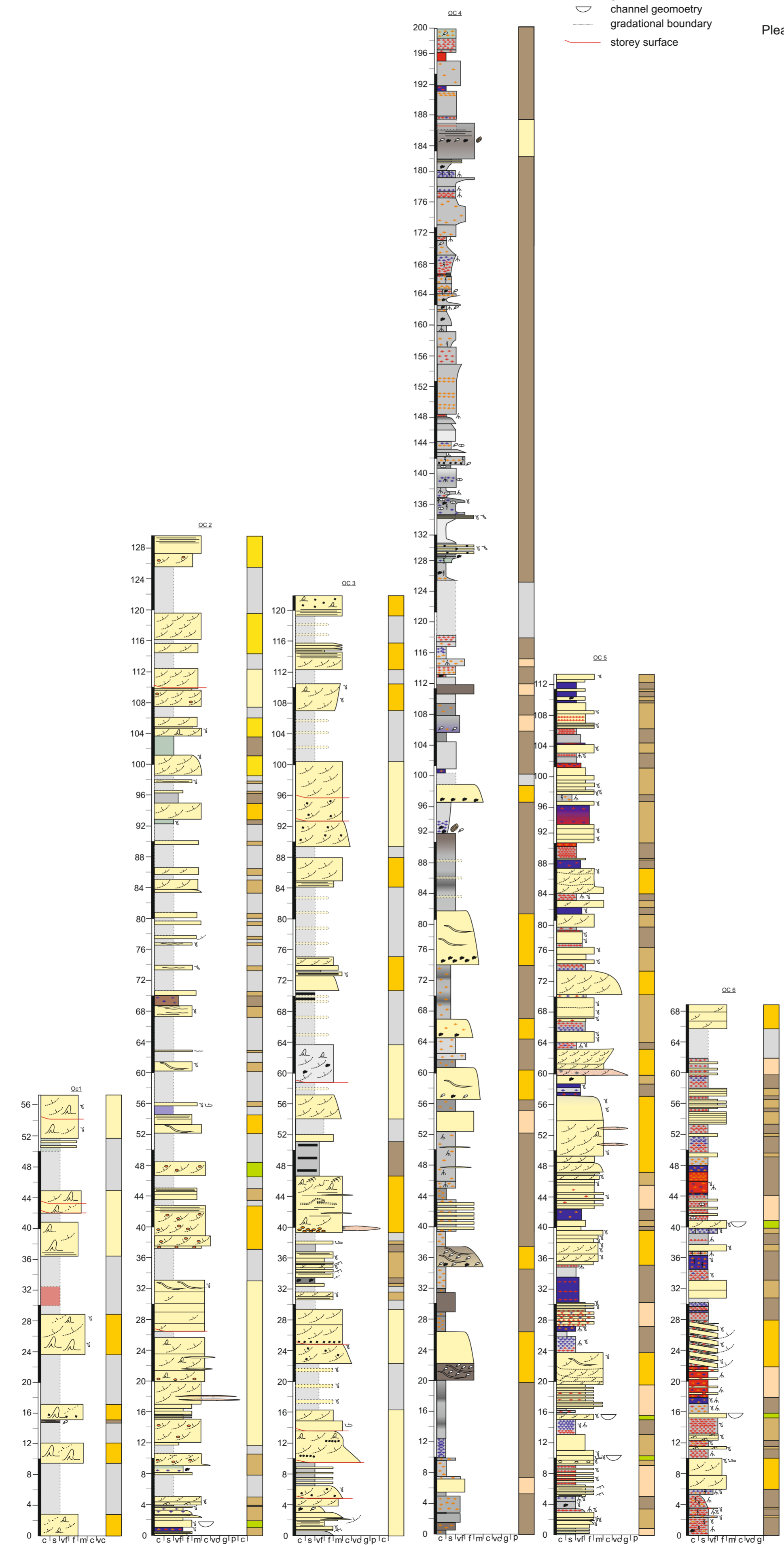


**Owl Creek System**

**KEY**

- |  |                           |  |                          |  |                                       |
|--|---------------------------|--|--------------------------|--|---------------------------------------|
|  | current ripples           |  | wood debris              |  | Massive channel facies                |
|  | horizontal lamination     |  | rootlets                 |  | Semi-Amalgamated channel facies       |
|  | trough cross-bedding      |  | vertical burrow          |  | Internally Amalgamated channel facies |
|  | wavy lamination           |  | sub-horizontal burrow    |  | Offset stacked channel facies         |
|  | slumping                  |  | horizontal burrow        |  | Isolated channel facies               |
|  | imbricated clasts         |  | groove                   |  | Floodplain - mud dominated            |
|  | accretion surface         |  | bone material            |  | Floodplain - sand dominated           |
|  | gravel lens               |  | shell material           |  | Floodplain - heterolithic             |
|  | sand lens                 |  | slickensides             |  | Floodplain channel (splay)            |
|  | soft sediment deformation |  | calcium carbonate nodule |  | Floodplain- inferred                  |
|  | mud clast                 |  | leaf material            |  |                                       |
|  | outsized clast            |  | mottling                 |  |                                       |
|  | granule                   |  | organic material         |  |                                       |
|  | channel geometry          |  |                          |  |                                       |
|  | gradational boundary      |  |                          |  |                                       |
|  | storey surface            |  |                          |  |                                       |

Please see Owen et al. 2017 for full facies descriptions



**Axial fluvial system**

**KEY**

- |  |                           |  |                          |  |                                       |
|--|---------------------------|--|--------------------------|--|---------------------------------------|
|  | current ripples           |  | wood debris              |  | Massive channel facies                |
|  | horizontal lamination     |  | rootlets                 |  | Semi-Amalgamated channel facies       |
|  | trough cross-bedding      |  | sub-horizontal burrow    |  | Internally Amalgamated channel facies |
|  | wavy lamination           |  | horizontal burrow        |  | Offset stacked channel facies         |
|  | slumping                  |  | groove                   |  | Isolated channel facies               |
|  | imbricated clasts         |  | bone material            |  | Floodplain - mud dominated            |
|  | accretion surface         |  | shell material           |  | Floodplain - sand dominated           |
|  | gravel lens               |  | slickensides             |  | Floodplain - heterolithic             |
|  | sand lens                 |  | calcium carbonate nodule |  | Floodplain channel (splay)            |
|  | soft sediment deformation |  | leaf material            |  | Floodplain - inferred                 |
|  | mud clast                 |  | mottling                 |  |                                       |
|  | oversized clast           |  | organic material         |  |                                       |
|  | granule                   |  |                          |  |                                       |
|  | channel geometry          |  |                          |  |                                       |
|  | gradational boundary      |  |                          |  |                                       |
|  | storey surface            |  |                          |  |                                       |

Please see Owen et al. 2017 for full facies descriptions

